Quantifying the Contributors to Extreme Sea Level Events in the Western Mediterranean at High Spatio-temporal Resolution

J. Ramos-Alcántara[1,2], M. Agulles[2], D. Gomis[2] and G. Jordà[1]

[1] Centre Oceanogràfic de Balears, C.N. Instituto Español de Oceanografía (CSIC), Palma de Mallorca, 07015, Spain.

[2] Institut Mediterrani d'Estudis Avançats, IMEDEA (UIB-CSIC), Esporles (Mallorca), 07190, Spain.

Corresponding author: Jorge Ramos Alcántara (jorge.ramos@ieo.csic.es), Gabriel Jordà (gabriel.jorda@ieo.csic.es)

Key Points:

- High frequency sea level records are needed to get a complete view of the processes contributing to extreme sea levels.
- Sub-hourly processes can be a major contributor to extreme levels in some locations, although they usually have a local scale.
- The contribution of waves to total sea level is highly dependent on the coastal morphology, and can lead to a rise of several meters.

Abstract

A comprehensive characterisation of extreme sea levels at different spatio-temporal scales is presented for the Western Mediterranean. The classical view of extreme sea levels as a consequence of the concurrence of storm events and high tides may lead to an incomplete picture for the Mediterranean coasts, where the tidal regime is small and processes operating at high frequencies can contribute significantly to extreme levels. Our approach bases on the analysis of tide gauge records with a high sampling frequency (1 minute), in order to consider other contributors beyond storm surges and tides. To have a basin-scale view, we first analyse the tide gauges operated by Puertos del Estado, which are distributed over all the Spanish Mediterranean coasts and cover at least from 2010 to 2022. Next, we focus on a more reduced domain to take advantage of the unprecedented spatio-temporal resolution of the VENOM tide gauge network, opering since 2020 in the Balearic archipelago. Last, we analyse the role of waves in local extreme sea level events by propagating waves towards the coast in the Bay of Palma. The wave run-up estimates are calculated considering the type of coastal protection and are used to simulate the potential flooding that could occur in the future under an unfavourable climate change scenario. Our results highlight the importance of high-frequency sea level records to study extreme events, and the key role of processes such as meteotsunamis and waves in the occurrence of extreme sea levels.

Plain Language Summary

Sea level extremes can cause significant environmental damage and affect the well-being of populations living in coastal regions. It is therefore essential to understand and quantify the mechanisms behind these extreme events. Storms are often considered to be the only cause of extreme sea levels; however, in this work we show that in some Mediterranean harbours there are other processes taking place at local scale and over short periods of time than can contribute to sea level extremes. We also show that the contribution of waves to coastal sea extreme elevations can be very significant, though it largely depends on the type of coastline. In particular, we show an example of the areas that could be flooded due to the wave contribution under an unfavourable scenario of sea level rise due to global warming. Overall, we show that for the study of extreme sea levels in the Mediterranean, using tide gauge series reporting at least

one datum per minute is essential, in order to consider the contribution of processes that are not usually taken into account.

1 Introduction

Extreme sea level events in coastal regions occur as a consequence of the overlapping of different processes that can act at different spatial and temporal scales. Extreme high waters can cause significant environmental damage and affect the well-being of populations living in coastal regions. Coastal flooding is one of the most common natural disasters (Noji, 1991) and can lead to erosion, damage to infrastructures and even loss of lifes (Ruggiero et al., 2001; Wolf, 2009). Moreover, in a context of global warming and projected sea level rise, the intensity of coastal impacts associated with extreme sea level events is expected to increase significantly (Nicholls et al., 2014; Wahl et al., 2017). In order to make proper assessments of the associated risks and hazards, it is necessary to characterise extreme sea level events, analysing in detail their spatio-temporal variability and quantifying the different processes contributing to extreme values (Del-Rosal-Salido et al., 2021).

In the Mediterranean coastal zone, the absolute magnitude of extreme events is small compared to other coastal regions, in part due to the microtidal regime of the basin (Muis et al., 2016). However, the microtidal regime also makes that coastal infrastructures are not as well adapted to large sea level anomalies as in other regions with larger tidal ranges. Furthermore, an important part of the economy of Mediterranean regions depends on coastal activities (e.g. tourism, trading and transport, ...), making this region particularly vulnerable to the consequences of extreme sea levels (Agulles et al., 2021; Gomis et al., 2012).

Coastal sea level variability results from the overlapping of many physical processes operating over a wide range of frequencies and spatial scales. Those taking place on long time scales (e.g. seasonal to multidecadal) are assumed to behave similarly in the coastal zone and in the open ocean. On the other hand, coastal areas are also affected by other contributions with shorter temporal and spatial scales, such as storm surges, seiches and wave runup (Woodworth et al., 2019). In practice, extreme sea level events are often quantified as the result of just two processes: tides and storm surges (Menéndez & Woodworth, 2010; Middleton & Thompson, 1986; Muis et al., 2016). However, up to our knowledge the accuracy of this approach has not

been assessed in the Mediterranean Sea, where there are clues suggesting the significant contribution of other processes.

One of the coastal phenomena that may contribute to Mediterranean extreme events are meteotsunamis, atmospherically-induced waves in the tsunami frequency band (2-120 min) that can cause considerable damage to infrastructure and ships (see e.g. Monserrat et al., 2006; Rabinovich, 2020). Vilibić & Šepić (2017) suggested that the contribution of such high frequency phenomena to extreme coastal sea level events could be of up to 50%. Another important driver of coastal sea level is the effect of waves reaching the coast, which can lead to an elevation of sea level over the still water level (referred to as wave runup). The wave runup is in fact the sum of the wave setup elevation onshore and the effect of swash fluctuations (Melet et al., 2018; Ruggiero et al., 2001). This phenomenon can be a dominant contributor in coastal extreme events causing overtopping of coastal infrastructures (Raby, 2003). Although Mediterranean wave heights are usually smaller than in the large oceans, their role can be important in extreme events such as the storm Gloria, in 2020, when the main impacts on the coast were caused by the large waves associated with strong winds (Amores et al., 2020; de Alfonso et al., 2021).

When high frequency processes play an important role, the characterization of extreme sea level contributors requires an adequate temporal sampling. Most of the studies undertaken so far have used hourly time series from tide gauges (see e.g. Calafat et al., 2009; Callahan & Leathers, 2021; Tsimplis & Shaw, 2010), mainly because few long records with a higher frequency sampling were available. However, the situation has changed in the recent years, and nowadays it is possible to find tide gauge datasets covering several years with a 1-min resolution (e.g. García-Valdecasas et al., 2021; Pérez Gómez et al., 2022). Another feature to be considered is that most tide gauges are located in sheltered harbours, where the wave set-up signal is diminished or practically not present; as a consequence, many of the operational tide gauges only record what is known as Still Water Level (SWLs) (Lambert et al., 2020; Melet et al., 2018). This makes that the only way to obtain a proper regional characterization of the wave effect on sea level is using numerical models (Holthuijsen, 2007).

The main objective of this paper is to understand and quantify the different mechanisms contributing to coastal extreme sea level events in the western Mediterranean. For this purpose,

we use 1-min tide gauge records altogether with outputs from storm surge and wave numerical models. The paper is organised as follows: in section 2, we describe the datasets and the methodology used to characterize the different contributors to extreme sea levels. Results are presented in section 3, and consist of a first general characterisation of Western Mediterranean extremes (Sect. 3.1) followed by the quantification of the different contributors (Sect. 3.2). Particular attention is paid to the quantification of sub-hourly processes (sampled by an ultra-dense network of tide gauges operating in the Balearic archipelago, Sect. 3.3) and to the contribution of waves to coastal flooding (for the particular case of the Bay of Palma, Sect. 3.4). Results also include an analysis of the spatial scale of each of the main contributors to extreme sea levels (Sect 3.5). Results are discussed in section 4 and the final remarks given in section 5.

2 Data and Methodology

2.1 Tide gauges records

Several sets of tide gauges with different time coverages have been used; in a first step we used data from tide gauges operated by Puertos del Estado, the Spanish holding of State Harbours (https://opendap.puertos.es/thredds/catalog.html). The REDMAR sea level network of Puertos del Estado operates 40 tide gauge stations and the network has been recently improved with the incorporation of new radar sensors that measure sea level at a frequency of 2 Hz (Pérez et al., 2013). From this dataset, the 17 stations located in the Mediterranean Sea (Fig. 1a) were selected and a minute time vector covering the period from 2010 to 2022 was defined (Table 1). In the framework of the VENOM project (acronym in Spanish of “Spatial Variability of Sea Level in the Western Mediterranean”), a low-cost ultra-dense and self-built tide gauge network has been recently deployed along the coasts of the Balearic Islands. The 20 VENOM tide gauges record sea level variations with a 1-min sampling rate, and add to other 12 tide gauges operated by other institutions and recording at the same frequency rate. Basing on the location, sampling rate and record length, we selected 21 tide gauges (listed in Table 2, Fig. 1b): 10 from the VENOM network, 5 operated by Puertos del Estado, 5 operated by the Balearic Islands Coastal Observing and Forecasting System (SOCIB: https://www.socib.es/, Tintoré et al (2013)) and 1 operated by Ports IB (http://webtrans.geonica.com). Altogether they constitute a network with an unprecedented high spatial density, which allows to investigate the small scale spatial variability of the different contributors to extreme sea level events. The resulting dataset has an average

Table 1: *Mediterranean tide gauges operated by Puertos del Estado, with their Location, Date of the first and last data of the considered series, and the Percentage of Missing Data.*

Station	Latitude(º)	Longitude(º)	First data	Last data	Missing values (%)
Tarifa	36.01	-5.60	01 January 2010	09 May 2022	6.47
Algeciras	36.18	-5.40	01 January 2010	09 May 2022	5.53
Málaga	36.71	-4.42	01 January 2010	09 May 2022	8.48
Motril	36.72	-3.52	01 January 2010	09 May 2022	6.58
Melilla	35.29	-2.93	01 January 2010	09 May 2022	9.83
Almería	36.83	-2.48	01 January 2010	09 May 2022	7.41
Carboneras	36.97	-1.90	25 April 2013	09 May 2022	7.89
Gandía	38.99	-0.15	01 January 2010	09 May 2022	4.36
Valencia	39.44	-0.31	01 January 2010	09 May 2022	7.77
Sagunto	39.63	-0.21	01 January 2010	09 May 2022	6.07
Tarragona	41.08	1.21	27 May 2011	09 May 2022	6.09
Barcelona	41.34	2.17	01 January 2010	06 May 2022	5.51
Ibiza	38.91	1.45	01 January 2010	09 May 2022	5.57
Formentera	38.73	1.42	22 January 2010	09 May 2022	8.59
Palma	39.56	2.64	01 January 2010	09 May 2022	16.45
Alcudia	39.83	3.14	01 January 2010	09 May 2022	11.30
Mahón	39.89	4.27	01 January 2010	09 May 2022	10.10

separation between stations of 8.7 km, in contrast with the average separation of the REDMAR tide gauge network in the Western Mediterranean, which is of 58.7 km. The first instruments of the VENOM network were installed at the beginning of 2020; the period used for the analysis performed in this work covers two years, from July 2020 to July 2022.

Tide gauge measurements are subject to errors of different nature that can affect the consistency and reliability of the series. Thus, a manual control was first applied to the series in order to detect and correct eventual discontinuities in the datum, and to discard out-of-range and other clearly anomalous values. An automatic quality control based on well-established procedures (see e.g. Reek et al., 1992; Williams et al., 2019) was subsequently applied. That second step included: (i) the elimination of values outside the interval defined by the average of each series ± 4 times the standard deviation; (ii) the identification of spikes through the analysis of the differences between groups of 3 consecutive measurements. Finally, the measurements that

passed this quality control were converted into sea level anomalies (SLA) by subtracting the temporal average of the corresponding series.

Table 2: *Selected tide gauges in the Balearic Islands, specifying the Institutions operating them, their Locations, the start and end Dates of the series and the Percentage of missing data.*

Station	**Institution**	**Latitude (º)**	**Longitude (º)**	**First data**	**Last data**	**Missing values (%)**
Formentera	Puertos del Estado	38.73	1.42	19 July 2020	19 July 2022	1.41
Sant Antoni	SOCIB	38.98	1.30	19 July 2020	19 July 2022	1.26
Ibiza	Puertos del Estado	38.91	1.45	19 July 2020	19 July 2022	2.55
Santa Eulália	VENOM	38.98	1.54	10 March 2021	06 July 2022	34.44
Sa Ràpita	SOCIB	39.54	2.38	19 July 2020	19 July 2022	4.49
S'Arenal	VENOM	39.50	2.75	22 January 2021	17 June 2022	39.38
Palma	Puertos del Estado	39.56	2.64	19 July 2020	19 July 2022	0.29
Palma	VENOM	39.56	2.64	21 January 2021	02 June 2022	31.97
Andratx	SOCIB	39.36	2.95	19 July 2020	19 July 2022	7.18
Port de Sóller	VENOM	39.80	2.69	19 July 2020	15 July 2022	11.50
Alcudia	Puertos del Estado	39.83	3.14	19 July 2020	19 July 2022	1.58
Can Picafort	VENOM	39.77	3.16	03 March 2021	13 July 2022	32.23
Colonia Sant Pere	SOCIB	39.54	3.34	19 July 2020	19 July 2022	34.56
Cala Rajada	VENOM	39.71	3.46	19 July 2020	17 March 2022	23.11
Cala Bona	VENOM	39.61	3.39	24 February 2021	19 July 2022	30.23
Porto Cristo	SOCIB	39.74	3.27	19 July 2020	19 July 2022	0.40
Portocolom	VENOM	39.42	3.26	19 July 2020	19 July 2022	0.87
Portopetro	VENOM	39.36	3.21	19 July 2020	19 July 2022	0.97
Mahón	Puertos del Estado	39.89	4.27	19 July 2020	19 July 2022	1.74
Ciutadella	Ports IB	39.99	3.83	19 July 2020	19 July 2022	0.19
Fornells	VENOM	40.05	4.13	19 August 2020	30 December 2021	33.58

2.2 Decomposition of sea level records

In order to assess the role of the different processes contributing to sea level extrems, the tide gauge time series were split into several components (Fig. 2):

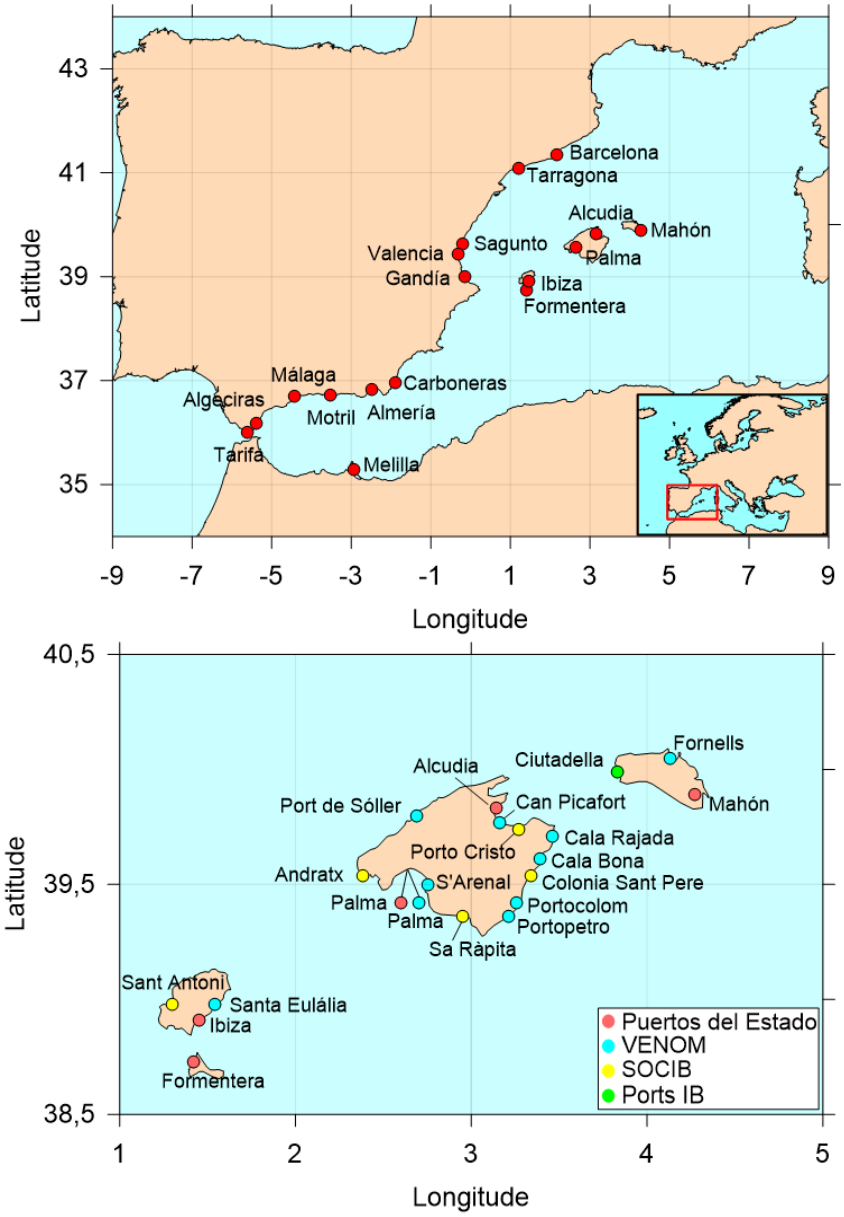

Figure 1: a) Location of the tide gauges from Puertos del Estado available in the Western Mediterranean, b) Location of the selected tide gauges in the Balearic archipelago, with the color indicating the institution operating them.

- **Atmospheric component:** Hourly sea level variations caused by changes in the atmospheric pressure and wind were obtained from the outputs of the NIVMAR forecasting system (Álvarez Fanjul et al., 2001), which are available from the website of Puertos del Estado (http://opendap.puertos.es/thredds/catalog.html). The NIVMAR system is based on the model HAMSON (Backhaus, 1985) forced by with wind and sea level pressure data provided by the

European Centre for Medium-Range Weather Forecasts (ECMWF, https://www.ecmwf.int/). The hourly time series were first converted into 1-min time series using a linear interpolation and then they were split into two frequency bands: T>1month and T<1month, which will hereafter be referred to as the low-frequency atmospheric contribution (T>1month) and the Storm Surge contribution (T<1month). It is important to note that this approach differs from other studies where the surge component is simply defined as the non-tidal residual of the original series, without further considerations on the forcing mechanisms of the observed sea level variability (Horsburgh & Wilson, 2007; Menéndez & Woodworth, 2010).

- **Seasonal cycle:** Seasonal sea level changes in the Mediterranean are mainly due to steric effects in the upper ocean (Gomis et al., 2012; Tsimplis & Woodworth, 1994) and to seasonal mass transports through the Strait of Gibraltar (Soto-Navarro et al., 2010). The seasonal cycle was obtained by interpolating to 1-min the monthly averages of the tide gauge records once the atmospheric component was removed.

- **Astronomical tide:** Once the atmospheric component and seasonal cycle were subtracted from the original series, the remaining sea level signal was adjusted by using the Matlab UTIDE functions (Codiga, 2023).

- **Residuals:** the residuals remaining after removing the previous components were separated into three frequency bands: T>1month, 1hour<T<1month, T<1hour. Although these bands do not correspond to specific physical processes, the main drivers of the variability of each band are known. The lower frequency band (T>1m) is mainly driven by the hydrodynamic structure of the Mediterranean basin (Larnicol et al., 2002) and by changes in the characteristics of the incoming Atlantic waters (Tsimplis et al., 2013). The high frequency band (T<1h) includes phenomena such as shelf waves or meteotsunamis, which can lead to resonant responses of remarkable magnitude in different inlets and bays of the Western Mediterranean (Monserrat et al., 2006). Finally, the intermediate frequency band (1h<T<1m) is the domain of other processes such as wave-induced variability or runoff from rivers (Huthnance et al., 1986; Melet et al., 2018; Woodworth et al., 2019).

An example of the splitting of a tide gauge record (Mahón) into the described components is shown in Fig. 2.

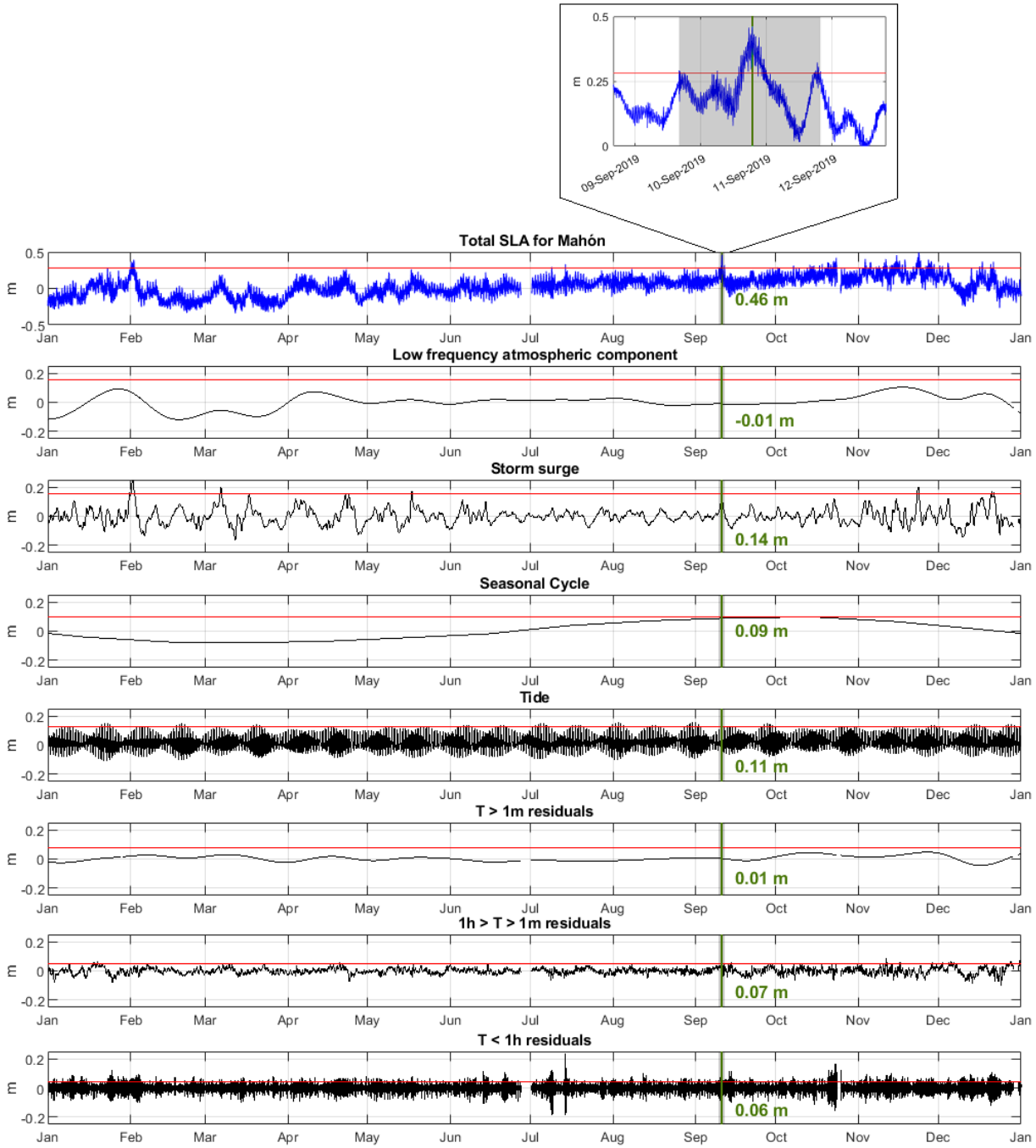

Figure 2: Component decomposition of the Mahón tide gauge record of 2019. For the total series and for each component, the 99th percentile has been marked with a red line. A particular extreme event is selected as example, indicating the time of its peak with a green line. The total sea level anomaly and the value of each component at the time of the peak is shown as green text. A zoom of this event is highlighted at the top of the figure.

2.3 Processing of extreme sea level events

Extreme sea level events were identified in the tide gauge series on the basis of their 99th percentile. Following the criteria of other authors (Calafat et al., 2014; Cid et al., 2016; Marcos & Woodworth, 2017), measurements over this threshold separated by less than 3 days were considered as a single event, in order to ensure the independence between events. After the identification, the main characteristics of the event (starting time, ending time, peak value, instant of maximum height and average value during the event) were determined. The duration of the event was determined as the time during which sea level was above the 99th percentile, between the starting and ending times of the event. Another interesting parameter is the intensity of the event, defined as the area between the series and the 99th percentile, integrated over the duration of the event. For this calculation we used the numerical integration method of the trapezoid rule (see e.g. Smyth, 2005).

To estimate return levels, we used the classical method of modelling exceedances over a threshold, through an Extreme-value distribution (Dupuis, 1999). The use of the extremes over a threshold is an appropriate alternative to modelling from the yearly maximum extremes, which can lead to a loss of information in the case that the extremes of any year are exceptionally low (Dey & Das, 2016; Marcos et al., 2009). Thus, if μ is the considered high threshold of a series (the 99.5th percentile in our case), the cumulative distribution function of the series of excesses $y = x - \mu$ can be approximated by the generalized Pareto distribution (GPD):

$$H(y) = 1 - \left(1 - \frac{\xi y}{\sigma}\right)^{-\frac{1}{\xi}} \quad (1)$$

where ξ is the shape parameter and σ (>0) is the scale parameter, both being estimated by maximum likelihood. In our case the shape parameter must be $\xi \leq 0$, otherwise the distribution would have no upper limit and the existence of values over the threshold would not be possible. Fitting the extreme values to a GPD allows the estimation of the 95% confidence intervals for the parameters of the distribution, which in turn enables to establish confidence intervals for the calculated return levels.

Return levels can be directly calculated from the parameters of the GPD distribution by means of the following expression:

$$R.L.(m) = \mu + \frac{\sigma}{\xi}\left(m^{\xi} - 1\right) \quad (2)$$

where R.L.(m) is the level expected to be exceeded once every m years. For each tide gauge, return levels were calculated both for the original series and for the separate components. Namely, for each component we analysed the reduction in return levels resulting from fitting the GPD distribution to the levels corresponding to the instants of the exceedances above the same threshold used for the original series, but after each component had been subtracted.

2.4 Quantification of the component contributions

The contribution of each of the identified components to the sea level anomaly series was quantified through the percentage contribution of each of them to the magnitude of the event peaks. If we consider for instance the event in the Mahón series highlighted in Fig. 2, the magnitude of the peak is 46 cm, and the component that contributes the most to it is the Storm Surge, whose series has a value of 14 cm at the instant of the peak. The contribution of that

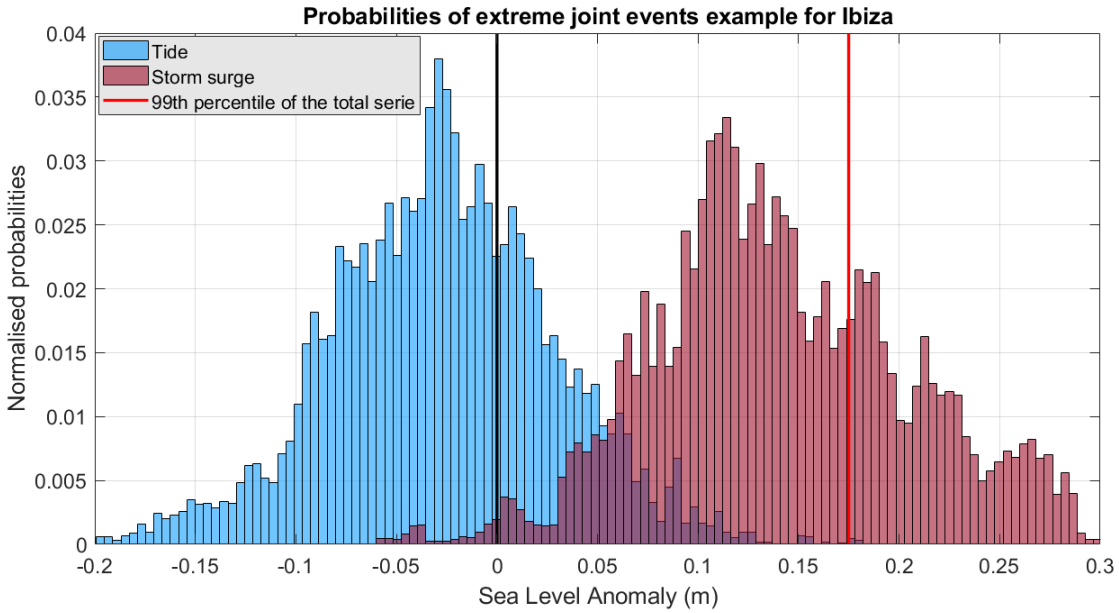

Figure 3: Probability distributions of extreme joint events derived from a synthetic series containing only the tidal and storm surge components.The black line marks the zero level of the total series, while the red line represents its 99th percentile.

component would then be evaluated in about 31%. The same procedure was applied to all the events.

The probability of extreme joint events was also estimated, as a measure of the dependence of extreme values with respect to each component (i.e., the probability of having an extreme value in a component and in the original SLA series at the same time). This probability can be calculated empirically through the percentage of extreme values of each component that coincide in time with extreme values of the total SLA series. For each component, a probability distribution function (pdf) of the total SLA is computed using the time intervals during which the component is above its own 99th percentile (i.e. when extreme values of that component are observed). If that pdf is centred around zero, this means that the component has no significant impact on the extremes of total SLA (i.e. extreme values of that component do not lead to extreme total SLA values). Conversely, if the pdf is displaced towards positive values, this means that extreme values of that component coincide with larger positive values of total SLA; that is, extreme values of that component significantly contribute to extreme SLA events.

For illustrative purposes, we have constructed a synthetic time series by adding only the tidal and storm surge components isolated from the Ibiza tide gauge. Given the microtidal regime of Ibiza, the extreme values of the total synthetic SLA will coincide with the extreme values of the storm surge component, while being independent of the tidal component. Figure 3 shows the synthetic total SLA pdf corresponding to extreme values of both, the tidal and storm surge components. For the tidal component, the distribution is centred slightly before the 0 level (black line), meaning that extreme values of the tides almost never translate into extremes of total SLA. On the contrary, extreme values of the storm surge component show a high coincidence with positive values of total SLA, and a substantial number of them (those to the right of the 99th percentile denoted by the red line) coincide with extreme values of total SLA. Therefore, in this example the storm surge would be the only responsible for the occurrence of extreme values of total SLA.

2.5 The role of wind waves

Although the contribution of wind waves to sea level within harbors is practically negligible, their contribution to extreme sea levels in exposed coasts can be very relevant. In order to

quantify this contribution, the wave runup 2% (hereafter RU2%), which corresponds to the characteristic value of 2% exceeding probability of individual waves reaching the swash zone during a sea state (Stockdon et al., 2006), was calculated along the coast of Palma Bay.

The contribution of waves to coastal sea level depends on the characteristics of the incoming offshore waves, but also (and critically) on the morphology of the coast (Dodet et al., 2019). The characterization of wave effects was carried out in two steps. First, the offshore wave regime of the period 2010 to 2022 was obtained from the SIMAR wave hindcast (Pilar et al., 2008) distributed by Puertos del Estado, which covers from 1958 to present. More specifically, the data belong to the WANA subset, which starts in 2006, and is based on WAM (Hasselmann et al., 1988) and Wavewatch (Tolman, 1991) models, forced by hourly wind fields provided by the Spanish State Meteorological Agency (AEMET). These offshore waves were then propagated up to the coast using the SWAN numerical model. SWAN is a third-generation shallow water model that solves the discrete spectral action balance equation (Booij & Holthuijsen, 1987) and has yielded accurate results in many studies (see e.g. Abu Zed et al., 2022). The model has been set up for the Palma Bay with a 100 x 100 m spatial resolution (Fig. 4), and uses the bathymetry grid obtained from GEBCO, the General Bathy-metric Chart Of Oceans (Weatherall et al., 2015).

Once the nearshore wave set-up and the wave climate was obtained at the control points (points 1 to 20 in Fig. 4), hourly sea state parameters (H_s and T_p) were used to calculate the RU2%. The estimation of RU2% depends on the coastal typology at each control point: where the coast is protected by artificial structures such as dikes or seawalls (magenta dots in Fig. 4), RU2% is estimated using an empirical formulations derived from laboratory experiments (Eurotop, 2018), while on beaches (white dots in Fig. 4) it is estimated using the empirical equation developed by Stockdon et al. (2006) and commonly used in coastal engineering studies (see e.g. Fiedler et al., 2018; Vousdoukas et al., 2012). For the beaches, we use the slope values estimated by Agulles et al. (2021) for the entire Balearic coastline, based on the equilibrium profiles.

In order to evaluate the impact of adding the wave contribution, we estimated the potentially flood-prone extension along Palma Bay, considering a mean sea level rise (MSLR) of 0.67 m, the regional value projected for the period 2080-2100 under the RCP8.5 scenario (Agulles et al., 2021; Cherif et al., 2020). On top of this MSLR, we considered 3 extreme sea level scenarios: i) the maximum sea level recorded by the Palma tide gauge (2010-2022), where wave effects are

minimal (ESC1); ii) the combination of the maximum recorded sea level (ESC1) with the wave set-up obtained at the control points (ESC2); iii) the combination of the maximum recorded sea level (ESC1) with the RU2% contribution obtained at the control points. The area flooded under each scenario was estimated by combining the "bathtub" approximation algorithm developed by Enríquez (2022) with the digital terrain elevation model developed by the Spanish National Geographic Institute, IGN (https://centrodedescargas.cnig.es/CentroDescargas/locale?request_locale=es). Although the "bathtub" approximation may be too simplistic to estimate the actual flooding caused by short events, it provides a useful first approximation to the impact of different definitions of extreme events.

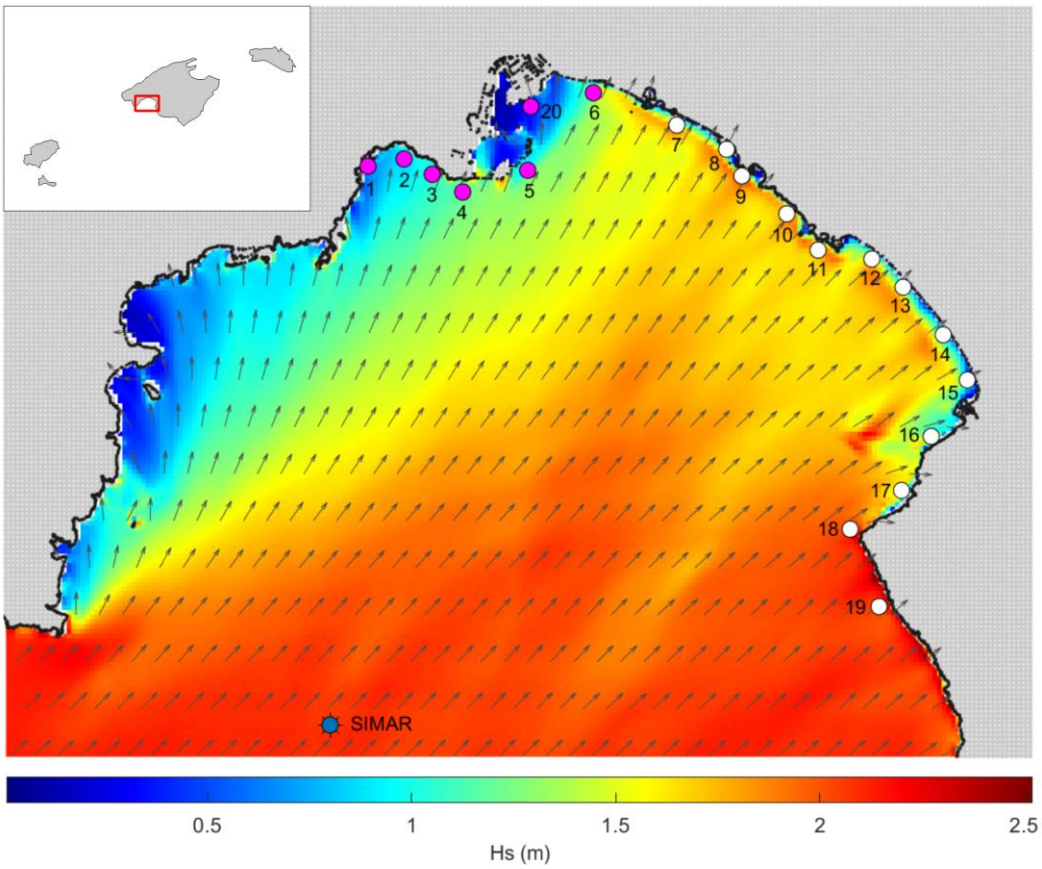

Figure 4: Example of the propagation of an offshore southwesterly sea state given at a SIMAR point (blue dot) towards the coasts of Palma Bay using the SWAN model. The control points where coastal waves are obtained are denoted by numbers from 1 to 20. The wave runup is calculated for artificial coastal protection (magenta dots) and on sandy beaches (white dots).

2.6 Spatial scales of the contributors to extreme events

To study the characteristic spatial scales of the different processes contributing to extreme sea level events, we calculated time correlations between the peak events identified at different stations for each component. But first, the time and intensity of the extreme values of each component had to be identified; we considered as independent events those separated by a minimum time lag that was set accordingly to the characteristic time scale of the component: 3 days for the total SLA series, 15 days for the low-frequency atmospheric component, 6 hours for the storm surge and half an hour for the sub-hourly residuals. Then, time correlation between all pairs of tide gauges were computed for each component; in order to allow for a certain time lag (i.e. the expected lag due to a moving storm), we considered the maximum value within a 1-day window around the date of each event. The result of the process is a set of correlation values (one for each pair of tide gauges) which are expected to show some dependence with respect to the separation distance between the instruments. Hence, fitting a spatial correlation function depending only on the separation distance $\rho(d_{ij})$, a characteristic length-scale L_s can be estimated. As spatial correlation model we used a Gaussian function (Rasmussen & Williams, 2008; Wilson & Adams, 2013):

$$\rho(d_{ij}) = exp(-0.5\, {d_{ij}}^2/{L_s}^2) \quad (3)$$

where d_{ij} is the distance between stations *i, j*.

3 Results

3.1 Overall characterization of extreme events

Figure 5 shows an overview of the peak values of the extreme events identified in the 17 tide gauge records covering the western sector of the Western Mediterranean and spanning the period 2010-2022 (see Table 1). Most of the medians of the peak values are between 30 and 40 cm, but they progressively increase for stations close to the Strait of Gibraltar. The reason for this behaviour is that the tidal regime of the Western Mediterranean is dominated by the M2 tidal component, which strongly reduces its amplitude after entering the basin through Gibraltar (Ferrarin et al., 2018). Therefore, the location of the station is expected to play a key role in the contribution of the tidal component to extreme events.

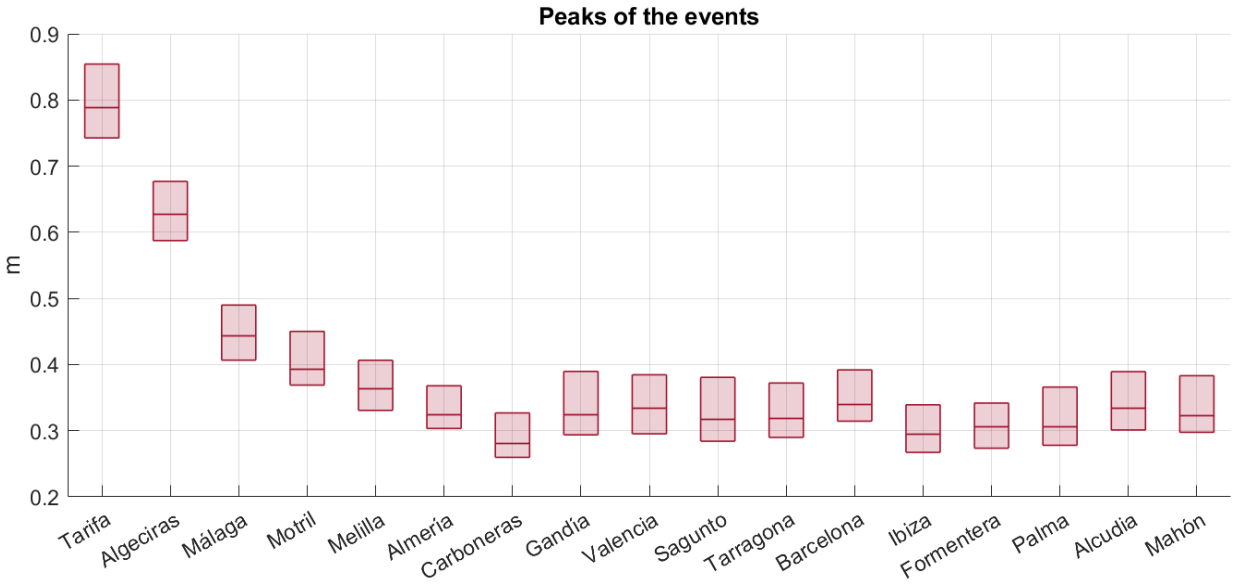

Figure 5: Peak values of the extreme events identified in the 17 tide gauge records spanning the period 2010-2022 (listed in Table 1). Boxplots report the median (inbox solid lines) and the 25th and 75th percentiles (bottom and top limit of the boxes).

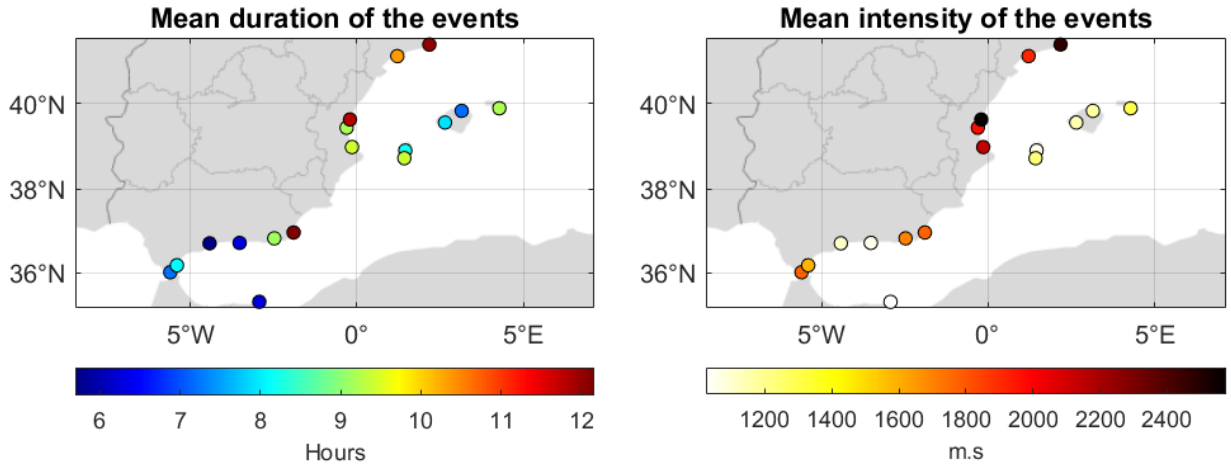

Figure 6: Mean duration (a) and mean intensity (b) of the extreme sea level events identified in the tide gauge records listed in Table 1.

Table 3: Additional information on the extreme sea level events identified in the tide gauge records of Table 1: maximum peak value, 99th percentile of the series, maximum duration, maximum intensity and 15-year return levels computed from hourly and minute series. The values in brackets of the last column are the % of increase with respect to the return levels computed from hourly series.

Station	99th percentile (m)	Maximum level (m)	Maximum duration (days)	Maximum intensity ($\cdot 10^3$ m·s)	Hourly 15-year return levels (m)	Minute 15-year return levels (m)
Tarifa	0.71	1.09	1.21	16.60	1.02	1.07 (5 %)
Algeciras	0.56	0.84	1.75	13.87	0.8	0.84 (5 %)
Málaga	0.39	0.71	3.22	25.59	0.63	0.75 (19 %)
Motril	0.35	0.62	3.12	18.99	0.55	0.66 (20 %)
Melilla	0.31	0.56	3.89	27.57	0.49	0.56 (14 %)
Almería	0.29	0.50	6.15	38.96	0.46	0.52 (13 %)
Carboneras	0.25	0.43	4.42	25.17	0.4	0.43 (8 %)
Gandía	0.27	0.44	6.36	56.78	0.4	0.44 (10 %)
Valencia	0.27	0.44	6.13	55.52	0.4	0.44 (10 %)
Sagunto	0.27	0.43	5.97	55.63	0.41	0.43 (5 %)
Tarragona	0.27	0.45	5.72	52.25	0.42	0.45 (7 %)
Barcelona	0.29	0.45	5.34	47.34	0.43	0.45 (5 %)
Ibiza	0.25	0.45	3.56	14.55	0.38	0.46 (21 %)
Formentera	0.26	0.47	7.33	30.77	0.4	0.46 (15 %)
Palma	0.26	0.46	4.69	18.22	0.41	0.48 (17 %)
Alcudia	0.28	0.49	5.30	24.59	0.43	0.49 (14 %)
Mahón	0.28	0.49	5.08	20.20	0.44	0.49 (11 %)

The duration and intensity of the identified extreme events is shown in Fig. 6. The mean duration ranges between 5.7 and 12.2 hours, with the largest values obtained in the northern sector of the Iberian peninsula coasts and the smallest values corresponding to stations near the Strait of Gibraltar (Fig. 6a). The mean intensity shows a similar pattern regarding the largest values, which exceed 2400 m·s for Barcelona and Sagunto stations; the smallest intensities correspond to the stations of the Balearic archipelago and the Alborán Sea (Fig. 6b).

Table 3 provides further information on the identified extreme events: the maximum peak value, the 99th percentile of the series, the maximum duration and intensity and the 15-year return levels are reported for each station. As expected, the maximum peak values correspond to the stations close to the Strait of Gibraltar; namely, the largest maximum for the considered period is

the 1.1 m obtained in Tarifa. The 99th percentiles, which are used as thresholds to identify extreme sea level levels, show a distribution similar to that of the maximum values, with a maximum of 0.71 m at Tarifa and a minimum of 0.25 m at Carboneras (southeast coast of the Iberian Peninsula). The maximum durations shows that sea level can be above the 99th percentile for more than 1 week (e.g. in Formentera). As it was the case for the mean duration, also the maximum durations are shorter close to the Strait of Gibraltar and larger at the northeast coast of the Iberian peninsula. The maximum intensities correspond to the east coast of the Iberian Peninsula, more precisely to the Gulf of Valencia, a region that is prone to the topographic blocking of storms coming from the East.

The computation of the monthly distribution of extreme events for each tide gauge of Table 1 (Fig. 7) confirms that they mostly occur in autumn, with October and November accounting for the highest number of events in almost all stations. The lowest occurrence is observed in late

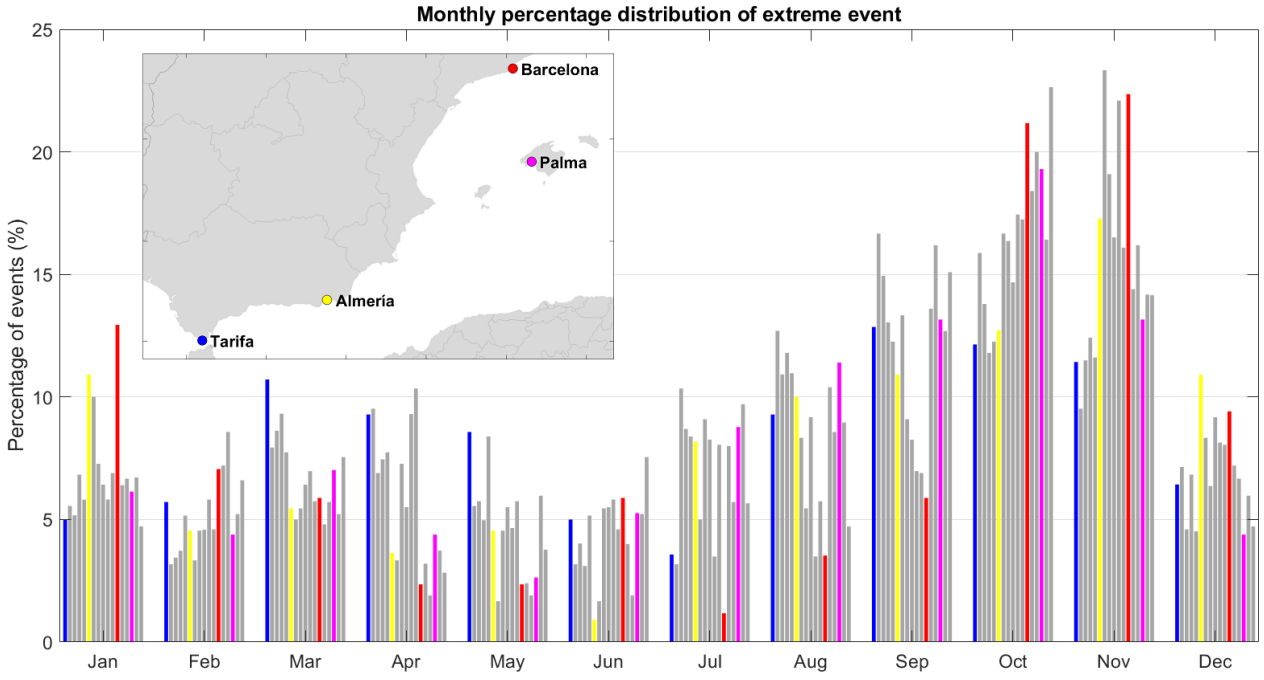

Figure 7: Monthly percentage distribution of extreme events in each tide gauge of Table 1. Four stations distributed throughout the basin (Tarifa, Almería, Barcelona and Palma) have been highlighted in colour.

spring and early summer. For the tide gauges located near the Strait of Gibraltar (Tarifa, Algeciras, Málaga, Motril, and Melilla), autumn is still the main season for extreme events, but the month with the highest occurrence is September. Moreover, the extreme events identified in these stations are more uniformly distributed throughout the year than for the stations located in the east coast of the Iberian Peninsula and the Balearic Islands.

A key feature revealed by Table 3 is the importance of using high frequency sea level series for studying extreme events. Comparing the return levels obtained from the minute and hourly series, the first exceed the second by an average of 6 cm. In relative terms, the increase in the return levels when using minute time series ranges between the ~5% of Tarifa, Algeciras, Sagunto and Barcelona to the ~20% of Málaga, Motril and Ibiza, the average increase being of about 11%.

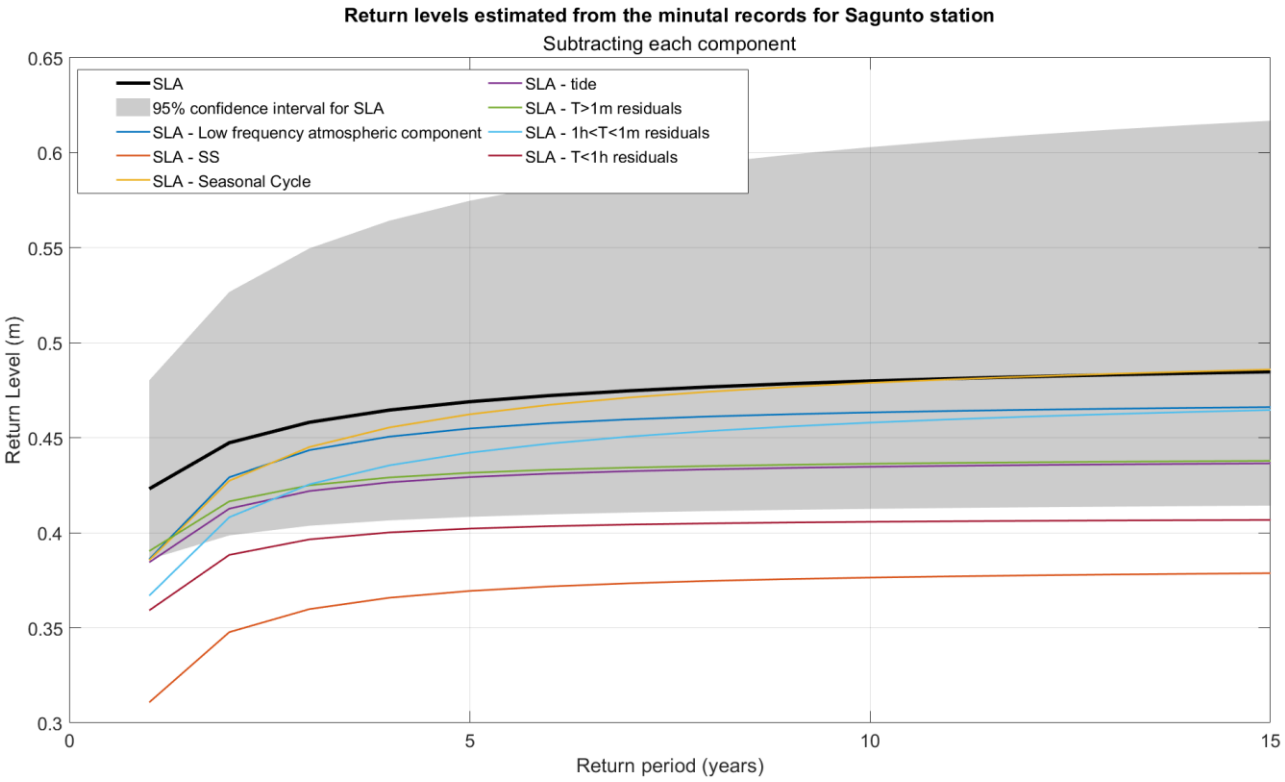

Figure 8: Estimated return levels for the Sagunto tide gauge. They are computed for the total SLA series and for the series resulting after the subtraction of each component. The grey area delimits the 95% confidence intervals of the original series return levels.

In order to highlight the importance of high-frequency processes, Fig. 8 shows the return levels computed for Sagunto, a tide gauge reporting large duration and intensity values but with the smallest difference between return levels computed from hourly series and minute series. The figure shows the return levels for the total SLA series and those obtained after subtracting each components from the total series. The decrease in the return levels observed after the subtraction of a components gives an idea of the relevance of that component. The largest reduction, slightly more than 10 cm, is obtained when subtracting the storm surge, and the second one, of the order of 7-8 cm, when subtracting the sub-hourly residuals. Removing the atmospheric signal with T>1 month reduces the return levels by about 5 cm, and subtracting the other components results is less relevant reductions. That is, high frequency (T<1h) processes are the second most relevant contributor to return levels even at the station with the smallest difference between return levels computed from hourly series and minute series. In general, the largest reductions in return levels are obtained when subtracting storm surge and high-frequency residuals at stations with a microtidal regime, whereas at those stations with a meso-tidal regime, the originally larger return levels are considerably reduced when subtracting the tide.

3.2 Contributors to the extreme events

The contribution of the tidal component is obviously very different between the stations with a meso-tidal regime (those located in the Alborán Sea) and the stations with a micro-tidal regime (those located on the eastern Iberian coast and the Balearic Islands). Therefore, when quantifying the different contributions of extreme sea levels the stations have been separated into two groups according to their tidal regime (Fig. 9). For the stations with a microtidal regime the most important contributions are atmospheric: the median values of the low frequency atmospheric contribution account for 5-14% of the peak values, while the median values of the storm surge account for 20-31% of the peak values. The contributions from sub-hourly periods also stands out as a relevant component, accounting for 8-24% of the peak values. For stations with a meso-tidal regime, the tide is by far the most important component, with a contribution that strongly depends on location: from the 88% of Tarifa (located just at the Strait of Gibraltar) to the 38% of Almería (located at the eastern boundary of the Alborán Sea). However, for an extreme event to take place, it is usually necessary that during neap tides some other component has a high value. The median contributions of the other components to peak values are: 1-5% from low frequency

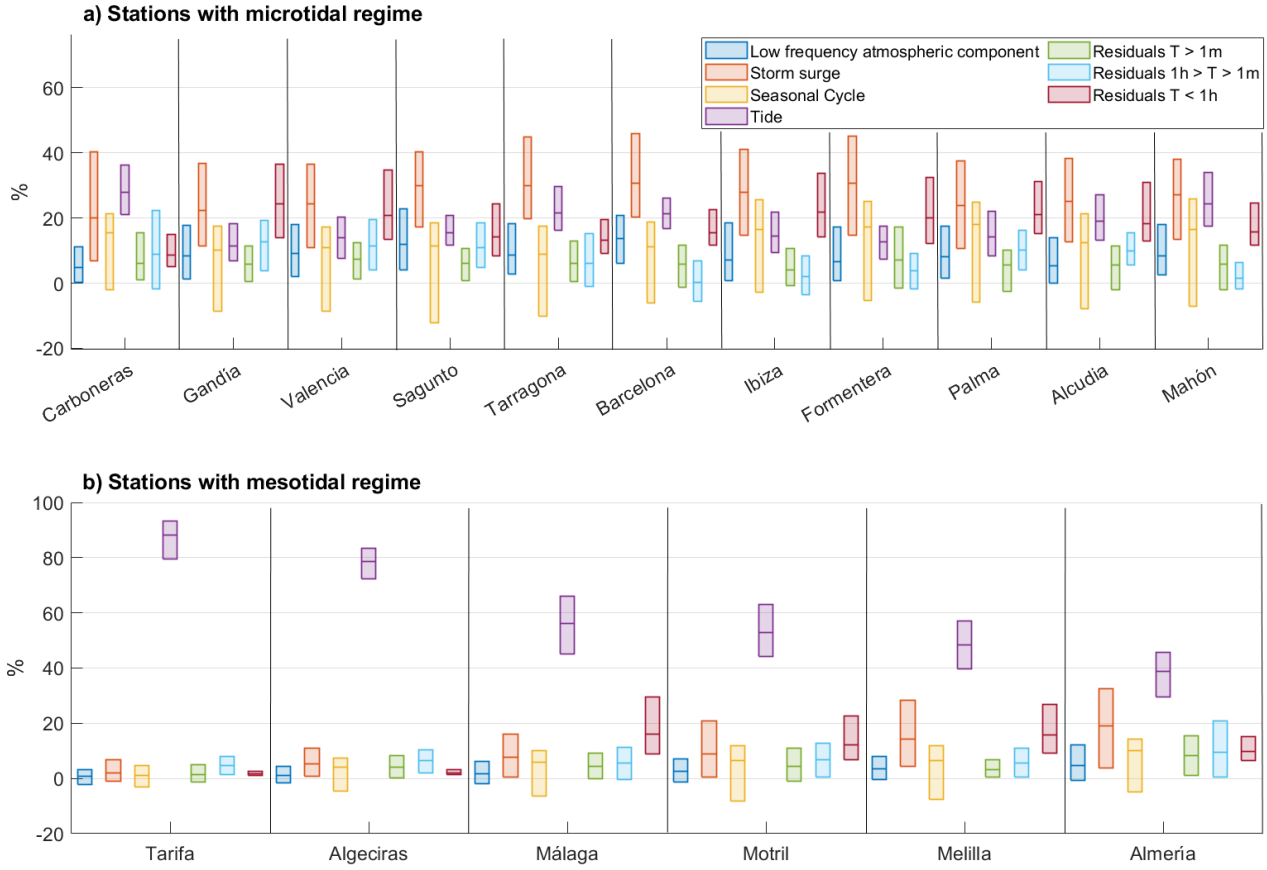

Figure 9: Percentage contributions of each sea level component to the peaks of extreme events identified in: a) tide gauges of Table 1 with a microtidal regime; b) tide gauges of Table 1 with a meso-tidal regime. Boxplots report the median (inbox solid lines) and the 25th and 75th percentiles (bottom and top limit of the boxes).

391 atmospheric processes, 2-19% from storm surges and 2-16% from high frequency (T<1h)
392 processes.

393 The relevance of each contributor can also be inferred from the probability of extreme joint
394 events distributions of total SLA and each component. As an example, Fig. 10 shows the pdfs
395 obtained for Palma de Mallorca, with the 0 level of total SLA marked in black and the 99th
396 percentile marked in red. For the case of Palma de Mallorca, the probability of having an
397 extreme value in the total SLA series is larger (18%) when there is an extreme value in the storm
398 surge component. However, the sub-hourly residuals (T<1h) are the second most important

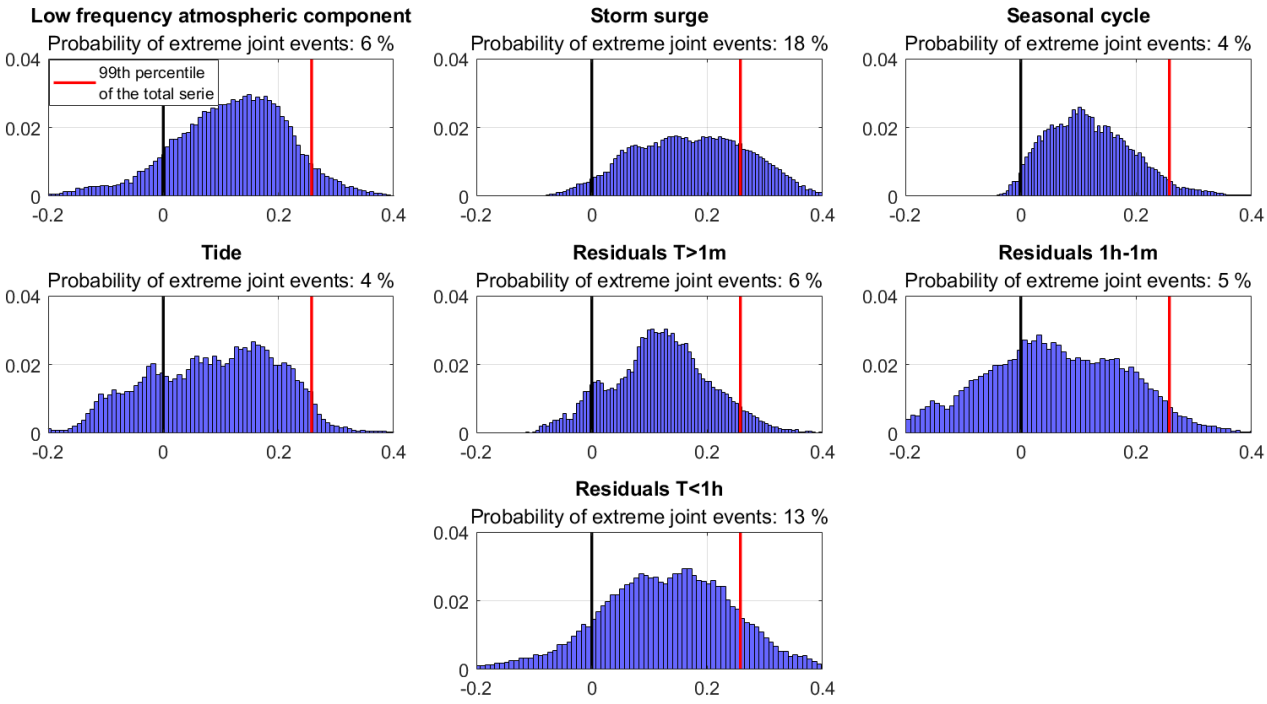

Figure 10: Probability of extreme joint events distributions of total SLA and each component for Palma de Mallorca tide gauge: a) Low-frequency atmospheric component; b) Storm surges; c) Tidal component; d) Seasonal cycle; e) Residuals with T >1m; f) Residuals with 1m<T<1h; g) Residuals with T<1h. The black line indicates the 0 level of total SLA marked and the red line indicates the 99th percentile.

399 component, with a probability of 13%. On the other hand, the probability that an extreme in the
400 total SLA series coincides with an extreme in the tidal and seasonal cycle components is of only
401 4% in both cases, indicating that these components have a limited impact in this station.
402 Nevertheless, it is worth noting that the distributions of all components are centred on positive
403 values, meaning that in general, the presence of extreme values in any component contributes
404 more or less to having high values in total sea level.

405 Figure 11 shows the results of applying the same analysis to all tide gauges of Table 1. The tidal
406 contribution is obviously crucial in the occurrence of extreme events near the Strait of Gibraltar.
407 However, the probability of extreme joint events of this component is about 55% at Tarifa, less

than 40% at Algeciras, and smaller at the other stations, indicating that although tides are the main contributor, high values of other components are also required for an extreme value to occur. At stations with a microtidal regime, the extremes in the storm surge have the highest probability of yielding a SLA extreme, with values ranging between 11.2 and 20.2%. The probability is also significant for subourly residuals, ranging from 5.6 to 13.3% and being particularly relevant at Gandía, Valencia and the Balearic Islands. The probabilities of the lower frequency residuals (T>1m and 1m<T<1h) are smaller and have an heterogeneous spatial pattern.

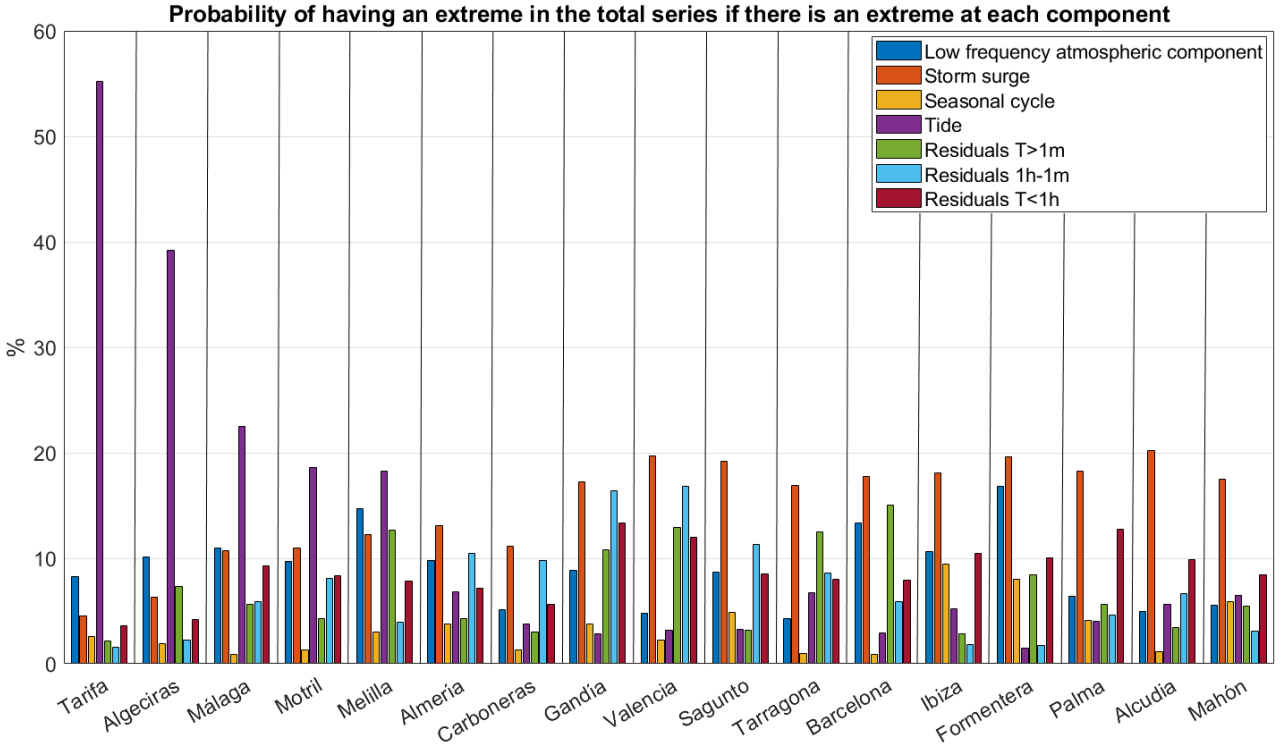

Figure 11: Probability of having an extreme event in the total SLA and simultaneously in one of the different contributors to sea level, estimated for each contributor and each tide gauge of Table 1.

3.3 Short-scale spatial variability of extreme events

As stated in Section 2, the recent availability of a tide gauge network with an unprecedented spatial resolution allows some insight into the short-scale spatial variability of extreme events. The analysis must however be taken with caution, as the short period spanned so far by the series

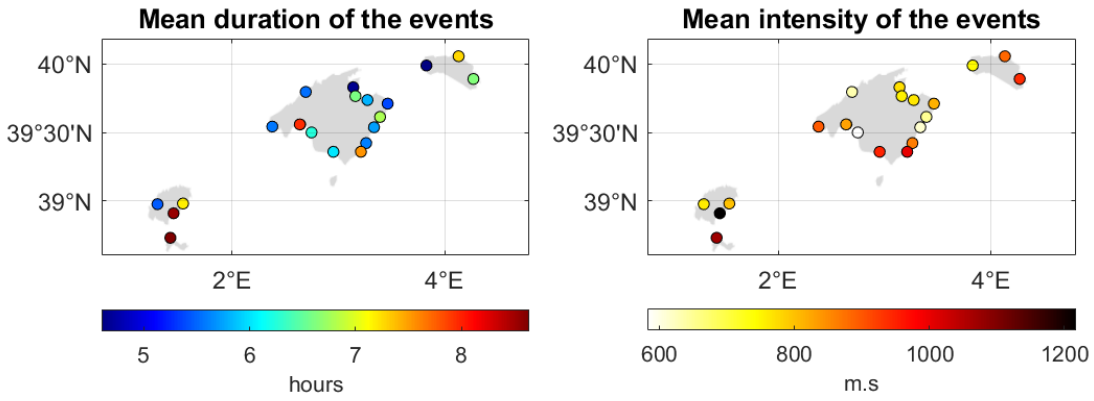

Figure 12: a) Average duration of extreme events in each station of the Balearic Islands, b) Average intensity of extreme events in each station of the Balearic Islands. Note that different colour maps have been used for each variable.

(2 years) does not allow a robust extreme value statistics. Figure 12 shows the mean duration (Fig. 12a) and mean intensity (Fig. 12b) of the extreme events identified for each tide gauge of Table 2. As a consequence of the short time period considered here, the five stations already used in Fig. 6 (in that case spanning more than 12 years) show similarities, but also some differenceswith respect to Fig. 12. Thus, the mean intensities of the events shown in Fig. 12 are considerably lower than those of Fig. 6, due to the smaller number of high level events in the series. Regarding the duration of the events (Fig. 12a), Palma, S'Arenal, Ibiza, and Formentera stand out, with a mean duration of more than 8 hours. The highest mean intensity corresponds to Ibiza, and amounts to ~1200 m·s. Table 4 shows additional information on the extreme events identified in each tide gauge record. The 99th percentiles are between 25 and 29 cm for all the stations, and the highest sea level value recorded in the region during the two-year period is the 73 cm recorded at Ciutadella. That location is well known for the occurrence of large amplitude sea level oscillations resulting from the resonant response of the harbour to incoming meteotsunami waves (locally known as “rissaga”, see e.g. Monserrat et al., 2006). The maximum duration and intensities are very heterogeneous throughout the stations, with the longest event lasting 3.5 days (in Sa Ràpita) and the most intense event amounting almost $18.7 \cdot 10^3$ m·s (in Andratx). Since the results obtained so far indicate that the contribution of sub-hourly processes can be quite relevant, the focus will now be put on the variability of this high-frequency

437 component in the regional context of the Balearic Islands (the domain covered by the dense
438 network of tide gauges).

439 Figure 13 shows the percentage contribution of sub-hourly processes to the peak value of the
440 extreme events identified in each tide gauge. Results show a marked heterogeneity, even for
441 stations separated a few kilometres. The stations with the highest contribution from this

Table 4: Information on the extreme events identified in each series in the Balearic Islands: maximum value reached, 99th percentile of the series, duration of the longest event recorded, and maximum intensity recorded for an event.

Station	**99th percentile (m)**	**Maximum (m)**	**Maximum duration (days)**	**Maximum intensity ($\cdot 10^3$ m·s)**
Formentera	0.25	0.43	1.9	9.69
Sant Antoni	0.26	0.55	1.58	7.98
Ibiza	0.25	0.48	2	10.47
Santa Eulália	0.25	0.54	2.37	7.01
Sa Ràpita	0.26	0.58	3.53	18.46
S'Arenal	0.29	0.49	1.41	2.9
Palma	0.25	0.52	3.04	15.2
Palma	0.28	0.43	1.5	4.44
Andratx	0.26	0.5	3.35	18.67
Port de Sóller	0.28	0.52	1.15	5.19
Alcudia	0.28	0.54	2	12.35
Can Picafort	0.28	0.58	1.18	3.73
Colonia Sant Pere	0.26	0.45	1.89	5.46
Cala Rajada	0.26	0.5	2.05	11.45
Cala Bona	0.27	0.41	1.22	2.81
Porto Cristo	0.27	0.56	1.59	8.46
Portocolom	0.27	0.64	2.61	13.1
Portopetro	0.25	0.47	1.97	9.78
Mahón	0.27	0.51	2.39	11.64
Ciutadella	0.28	0.73	1.57	8.56
Fornells	0.26	0.4	1.55	6.8

component are Ciutadella, with a 53.5%, Portocolom with 47.3%, Port de Sóller, with 42.1%, and Sant Antoni, with 40.7%. All them have at least one event in which the contribution of this component is greater than 100%, indicating that it is the only responsible for these events (and that it compensates the negative levels associated with other components). These stations are all located in sheltered harbours where meteotsunami episodes are relatively frequent (Rabinovich, 2020). On the other hand, there are stations where the contribution of this component is very small, such as Fornells, Port de Valldemossa or Sa Calobra; these stations are located in places where neither shelf nor harbour resonance have been reported.

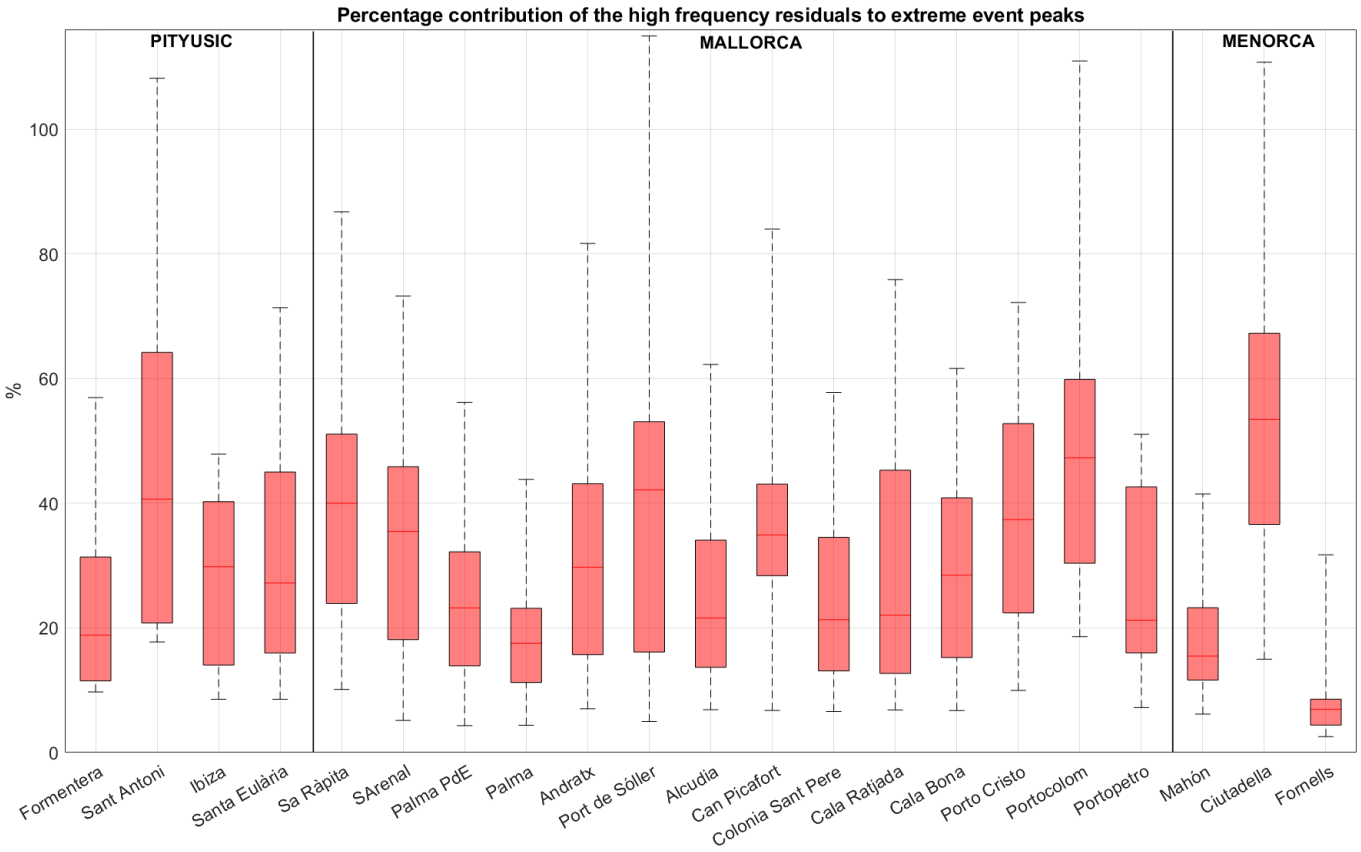

Figure 13: Percentage contributions of high-frequency residuals (T<1h) to extreme sea levels in the Balearic Islands. The stations are separated by islands: Pityusic (Ibiza and Formentera), Mallorca and Menorca. Boxplots report the median (inbox solid lines) and the 25th and 75th percentiles (bottom and top limit of the boxes). The whiskers represent the minimum and maximum values of the contribution of this component to the extremes of each series.

3.4 Wave contribution to extreme events

Here we present the results of the wave contribution to Total Water Level (TWL) at the 20 control points shown in Fig. 4. The maximum value measured by the Palma station operating with 1-min resolution is 46 cm; the tide gauge is located in the vicinity of point 20 (see Fig. 4), and it can be considered representative of the sea level of the whole bay without considering the wave contribution. When the set-up contribution is added, then TWL reaches values between 0.46 and 0.49 m over artificial coastal structures (points 1-6 and 20), and between 0.46 and 0.78 m on the beach (see Table 5). When the RU2% contribution is considered, then TWL reaches

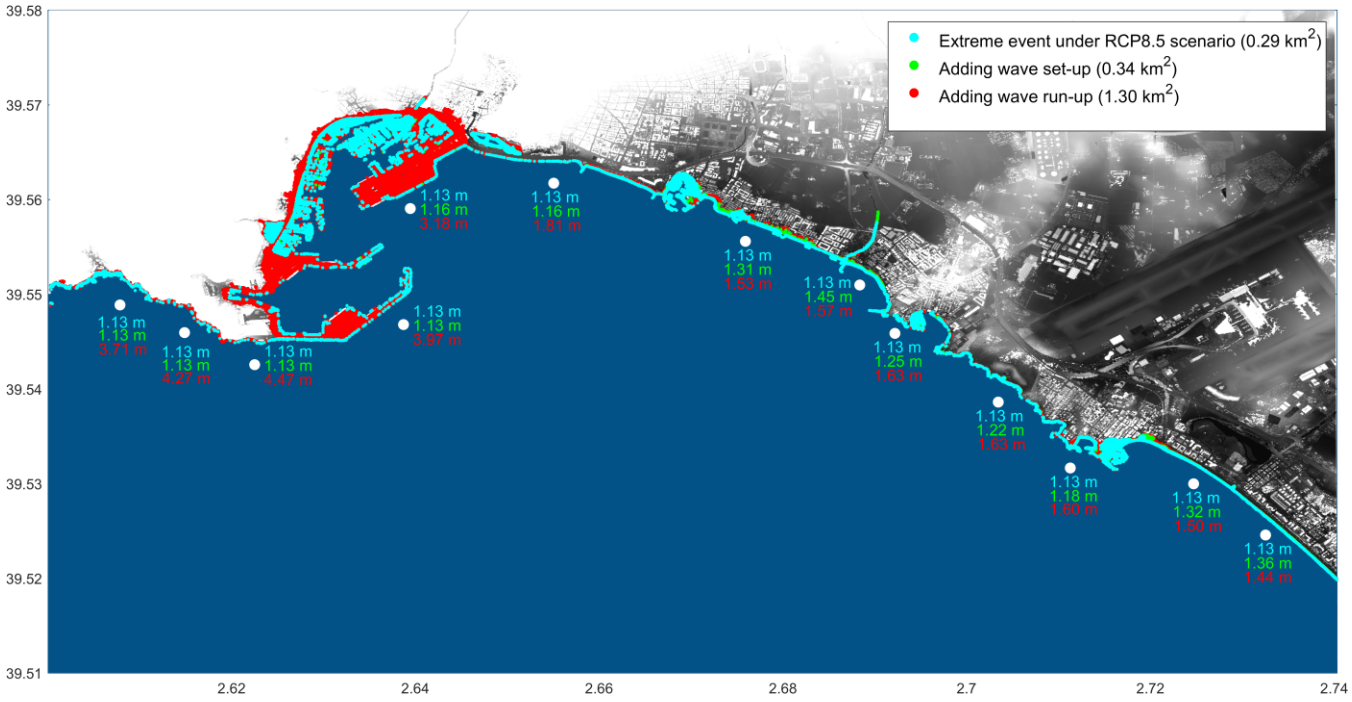

Figure 14: Potentially flood-prone areas of Palma Bay during an intense extreme event occurring under the RCP8.5 scenario projected for the end of the century (2080-2100). Cyan areas are those flooded without considering the wave contribution, green areas are those flooded when considering the wave set-up contribution, and red areas are those impacted when adding the RU2% contribution. The vertical values of sea level at each control point (TWL) are also given with and without the wave contribution.

Table 5: Total Water Level (TWL) at the 20 shore points of Palma Bay shown in Fig. 4. It includes the TWL when adding the wave set-up, provided by the SWAN model, and the TWL calculated when adding the estimated wave run-up contribution, both considering the maximum level recorded at Palma tide gauge (0.46 m); the type of coastal protection and the parameterisation used in the calculation of the RU2% are indicated for each point. Future TWLs would be obtained by adding a mean sea level rise of 0.67m (the regional value projected for 2100 under the RCP8.5 scenario) to present TWLs.

Control point	Coastal typology	TWL when adding set-up (m)	TWL when adding RU2%	
			Source	Value (m)
1	Dike	0.46	Eurotop	3.29
2	Dike	0.46	Eurotop	3.04
3	Dike	0.46	Eurotop	3.60
4	Dike	0.46	Eurotop	3.80
5	Dike	0.46	Eurotop	3.30
6	Dike	0.49	Eurotop	2.51
7	Beach	0.64	ST2006	0.86
8	Beach	0.78	ST2006	0.90
9	Beach	0.58	ST2006	0.96
10	Beach	0.55	ST2006	0.96
11	Beach	0.51	ST2006	0.93
12	Beach	0.65	ST2006	0.83
13	Beach	0.69	ST2006	0.77
14	Beach	0.67	ST2006	0.75
15	Beach	0.63	ST2006	0.73
16	Beach	0.48	ST2006	0.79
17	Beach	0.48	ST2006	0.90
18	Beach	0.46	ST2006	1.00
19	Beach	0.46	ST2006	1.00
20	Vertical	0.49	Eurotop	1.14

values between 1.14 and 3.80 m over artificial coastal structures (points 1-6 and 20), and between 0.73 and 1.00 m on the beach. The contribution of waves is therefore very relevant, specially in the artificial parts of the shore, where TWL can exceed the maximum tide gauge value by more than 3 m. It is worth noting that set-up contribution typically lasts as long as the

462 storm duration is (~hours), while the maximum values associated with the RU2% have a
463 duration determined by the wave period (~10 secs).

464 The contributions of the wave set-up and the RU2% have been considered separately, as their
465 durations are different: whereas set-up leads to a more persistent total level rise over the duration
466 of the storm, the RU2% generates a periodic vertical elevation with the period of incoming
467 waves. This makes that the coastal areas reached by the set-up can be effectively flooded;
468 conversely, the flow associated with the RU2% is too small as to flood all the area predicted by
469 the bathtub approximation, even if the effect of the swash in storms can be a major hazard in
470 coastal regions. Under the RCP8.5 scenario, future TWL would be equal to present values plus
471 0.67 m, the mean sea level rise projected for the end of this century. Under that scenario, the
472 potentially floodable areas of Palma Bay during an intense extreme event are shown in Fig. 14.
473 When the contribution of waves is not considered, the floodable area along the bay coast is 0.29
474 km^2. When adding the estimated wave set-up, the potentially floodable area increases up to 0.34
475 km^2, that is, an additional 17%. The impacted area when considering the runup is 1.30 km^2,
476 which is an increase of almost 350% over the area covered by the still water level.

477 3.5. Spatial scale of main contributors

478 The spatial scales of the extreme sea level events identified in the total series, and of the extreme
479 values of the main contributors to these events are inferred from Fig. 15. This Figure shows, for
480 all station pairs, the correlation between the time sequence of peaks identified at each station.

481 The correlations between station pairs have been computed for the total series (Fig. 15a), the low
482 frequency atmospheric component (Fig. 15b) and the storm surge component (Fig. 15c), and are
483 represented in all cases as a function of the distance between the two stations. The stations
484 considered for the referred components are the 17 tide gauges listed in Table 1, which result in a
485 total of 136 station pairs. For the sub-hourly residuals (T<1h), which are expected to have a
486 shorter spatial scale, the stations considered are the 21 tide gauges located in the Balearic
487 archipelago (listed in Table 2); in this case the number of correlation values between station pairs
488 is 210 (Fig. 15d).

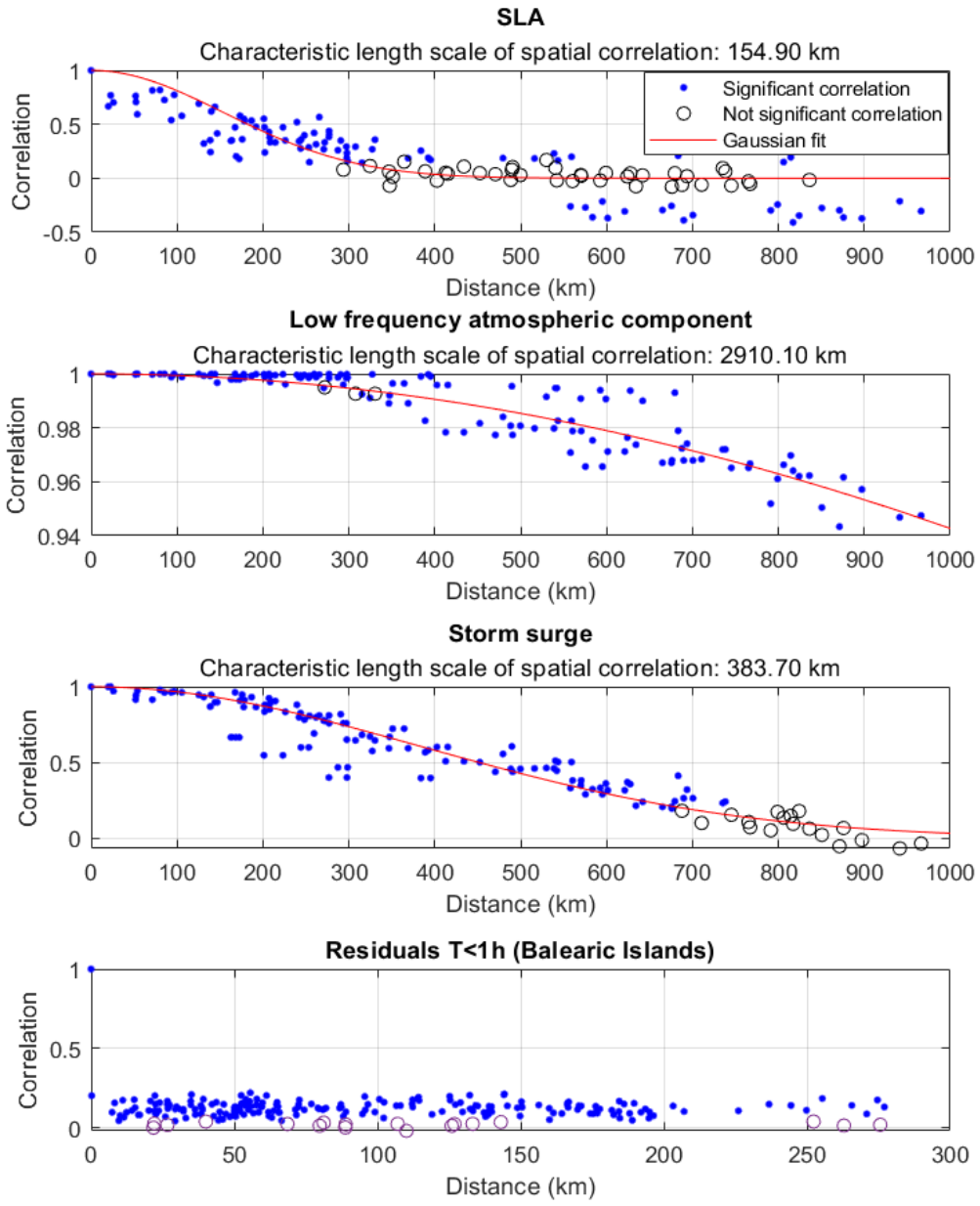

Figure 15: Correlation between the time sequences of peak values identified at each station pair. The correlation value obtained for each station pair is plotted as a function of the distance between the two stations in the form of a blue square (when the correlation is statistically significant) or an empty circle (when the correlation is not statistically significant). The procedure has been applied to the Western Mediterranean tide gauges of Table 1 (spanning the period 2010-2022) for: a) the total SLA series; b) the low frequency atmospheric component; c) the storm surge component; and to the Balearic Island tide gauges of Table 2 (spanning the period 2020-2022) for: d) the subhourly component. Note that the x-axis (distances) of panel d) are different from the other three panels.

For the extreme events of the low frequency atmospheric component and of the storm surge component, the fit of Eq. (3) to the significant correlations resulted in characteristic scale values of about 2900 km and 380 km, respectively. These values are consistent with the typical scales of the perturbations generating the extreme sea levels associated with these components. The characteristic scale obtained for total SLA is about 150 km; in this case, extreme values result from the overlapping of different processes with different scales, so that the value of 150 km must be considered a sort of average scale. The correlations obtained for the sub-hourly component are in general very low, regardless of the distance between stations, which prevents the estimation of a meaningful characteristic length scale for this component.

4. Discussion

A major objective of this work was to revisit the characteristics of extreme sea level events in the Western Mediterranean in the light of tide gauge data with a high spatio-temporal resolution. The importance of extreme events in that region is demonstrated by their duration (the time during which sea level remains above the 99^{th} percentile during the event), which can be of more than one week during intense events.

The sampling rate of tide gauges has often been a limiting factor for the identification of the actual magnitude of the peaks, since relevant high-frequency processes remain undersampled when using hourly records, for instance. Thus, previous works had already anticipated that the estimated return levels would increase if working with sea level series with a sampling period smaller than 1 hour (Tsimplis et al., 2009). Here we have shown that 15-yr return levels do indeed increase, namely between 5% to 20%, when working with minute series instead of hourly series. In terms of physical processes, missing the contribution of high frequencies to extreme sea levels leads to an overestimation of the importance of other contributions such as storm surges, to the point that the latter are often considered the only process responsible for extreme values.

A second, related objective of the work was the quantification of the contribution of different physical processes to extreme events. In many works, the residuals of de-trended and de-tided hourly series are directly considered as storm surges (see e.g. Enríquez et al., 2020; Haigh et al., 2016; Marcos & Woodworth, 2017). Here, we have split the total SLA series into different

contributions beyond tides and storm surges, finding that the de-tided residuals of the series after removing the steric and the atmospheric component can significantly contribute to the extreme levels, at least in some cases and at some stations. In fact, at many coastal sites with a micro-tidal regime (the whole Western Mediterranean except the Alborán Sea), sub-hourly processes (which include for instance meteotsunamis and shelf waves) are the second most important contributor to extreme levels, storm surges being always the main contributor. It is also worth noting, that even if storm surges are the main contributor, they contribute to 20-30 % of the peak level, which enforces the idea that extreme events require multiple contributions from different mechanisms.

The deployment in the Balearic Islands of a tide gauge network with an unprecedented spatio-temporal resolution has allowed a further insight into the contribution of sub-hourly residuals to extreme levels. It has been shown that high frequency processes ($T< 1$ h) are a key factor in the occurrence of extreme events in some ports, and that they are often absolutely local processes. In this sense it is worth noting that the conventional tide gauge networks (i.e. with less spatial resolution), may be unadequate to assess the importance of those events.

A third key feature of the study has been the evaluation of the impact that waves can have on total sea levels measured at the coast. The contribution of waves is highly dependent on the morphology of the coast (e.g., the estimated wave runup is considerably higher in the presence of rigid structures than on beaches) and on the orientation of the coastline with respect to the direction of the waves. Namely, our case study for the Bay of Palma has shown that during an intense event, sea level at coastal sites with artificial structures can be up to 2.5 m higher than in neighbouring sites with a beach-type morphology. Therefore, the approach followed in some works in which the wave runup is quantified without a detailed consideration of the coastline or coastal structure (see e.g. Melet et al., 2018; Sayol & Marcos, 2018) may be too simplistic. On the other hand, it should also be noted that those extreme values would occur over short periods (~secs), as they are associated to the swash part of the wave runup. Thus, the flood-prone areas shown in Fig. 14 constitute only a first illustrative approximation, as the bathtub approach tends to overestimate the extent of the flooded area.

Finally, regarding the characteristic spatial scale of the main contributors to extreme levels, it seems clear that the atmospheric contribution operates over a wide range of spatial scales: from

~3000 km in the case of the low frequency atmospheric component to a few km in the case of the resonant response of shelfs and harbours. In fact, the inference of a characteristic scale for the subhourly residuals has not been possible, even using a tide gauge network with a mean separation distance of ~10 km in large parts of the domain. The characteristic scale of storm surges has been quantified in 380 km, a value that differs significantly from the results given in other studies. Thus, Enríquez et al. (2020), who also estimated the spatial footprints of storm surges in the Western Mediterranean, obtained a coastal correlation length of 830 km (using a clustering analysis technique) and cluster lengths between 2000 and 3500 km (using the match level analysis and copula analysis methods). The differences are likely due to the fact that Enríquez et al. (2020) considered as storm surge all non-tidal residuals; this includes the low-frequency atmospheric component, which has been analysed separately in our work and for which we have obtained a characteristic scale of a few thousand km.

5. Conclusions

In this work we have provided a detailed description of the extreme events observed by tide gauges deployed on the coasts of the Western Mediterranean basin. We have analysed different time scales separately, in order to characterise and quantify the different processes that contribute to the occurrence of extreme sea levels on the coast. The different tidal regimes of the analysed domain condition the magnitude of extreme levels and determine at least in part the relative importance of the different components of extreme events. A feature common to the whole domain is that Autumn is clearly the season with the highest occurrence of extreme events.

A main conclusion of this work is that the availability of sea level records with a high sampling rate is of paramount importance for the study of extreme levels. Records with a 1-minute sampling interval allow a better identification of the contributors to coastal extreme sea level and a more accurate estimation of the maximum value of the peaks. In fact, they allow taking into account processes that are usually not considered in previous works using hourly time series.

For the stations of the Western Mediterranean with a microtidal regime, the main contributors to the extreme values are the storm surge, the low frequency component of the atmospheric contribution, and the sub-hourly processes. The tidal contribution is more important close to the Strait of Gibraltar, but still requires peaks in other components for an extreme to occur. The high

spatio-temporal resolution resulting from the deployment of the VENOM tide gauges (altogether with the tide gauges operated by other institutions in the Balearic Islands) has allowed a further insight into the contributions of sub-hourly processes to extreme sea levels. We have shown that these processes have a very small spatial scale, but they can nevertheless be very important at certain locations, becoming eventually the main contribution. The ports where this contribution is most important coincide with those places where meteotsunamis are usually reported, indicating that these phenomena are the dominant processes of the sub-hourly domain.

Finally, we have shown that waves can play a key role in the total water level reached during extreme events, as they can lead to a rise of several meters. The contribution of waves to coastal sea level is highly dependent on the type of coastal structure, reaching considerably higher values when they imping on rigid protections. As an application, we have obtained a first approximation to potentially flood-prone areas of the Bay of Palma during extreme events. The methodology applied to propagate the waves and obtain the flooding areas could be extrapolated to other regions. By adding the mean sea level rise projected under future climate scenarios, they constitutes a useful tool for stakeholders dealing with the coastal adaptation to climate change.

Acknowledgments

This work is part of the R+D+I coordinated project VENOM (PGC2018-099285-B-C21, PGC2018-099285-B-C22) and the project UNCHAIN (PCI2019-103680), both funded by MCIN/AEI/10.13039/501100011033 and by the ERDF (A way of making Europe). This research has been supported by the Ministerio de Ciencia e Innovación and the European Regional Development Fund, Interreg. We thank the data providers (Puertos del Estado, SOCIB and Ports-IB) for making their datasets freely available. We also want to thank the support of the Balearic Holding of Harbours (Ports-IB) to the deployment of the VENOM tide gauge network and all the members of the Sea Level and Climate group that have participated in the design, installation and maintenance of the network, particularly Joan Puigdefabregas, Aida Frank-Comas, Joan Villalonga, Joaquim Tomàs-Ferrer, Albert Font and Javier Soto-Navarro.

Open Research

The data of the REDMAR tide gauges network of Puertos del Estado are accessible through its web catalogue (https://opendap.puertos.es/thredds/catalog.html, last accessed 9 february 2023, Pérez et al., 2013). In the same catalogue the outputs of the NIVMAR forecasting system (https://opendap.puertos.es/thredds/catalog/nivmar_large_nivmar/catalog.html, last accessed 9 february 2023, Álvarez Fanjul et al., 2001) are also available. The wave parameters of the SIMAR wave hindcast can be consulted on the web page of Puertos del Estado (https://www.puertos.es/es-es/oceanografia/Paginas/portus.aspx, last accessed 9 february 2023, Pilar et al., 2008). The bathymetric grid used for the shoreward wave propagation was obtained from the GEBCO website (https://www.gebco.net/, last accessed 9 february 2023, Weatherall et al., 2015). The code developed to identify and analyse the extreme events of the tide gauge series can be accessed at https://doi.org/10.5281/zenodo.7848818 (Ramos-Alcántara et al., 2023).

References

Abu Zed, A. A., Kansoh, R. M., Iskander, M. M., & Elkholy, M. (2022). Wind and wave climate southeastern of the Mediterranean Sea based on a high-resolution SWAN model. *Dynamics of Atmospheres and Oceans*, *99*, 101311. https://doi.org/10.1016/j.dynatmoce.2022.101311

Agulles, M., Jordà, G., & Lionello, P. (2021). Flooding of Sandy Beaches in a Changing Climate. The Case of the Balearic Islands (NW Mediterranean). *Frontiers in Marine Science*, *8*, 760725. https://doi.org/10.3389/fmars.2021.760725

Álvarez Fanjul, E., Pérez Gómez, B., & Rodríguez Sánchez Arévalo, I. (2001). Nivmar: A storm surge forecasting system for Spanish waters. *Scientia Marina*, *65*(S1), 145–154. https://doi.org/10.3989/scimar.2001.65s1145

Amores, A., Marcos, M., Carrió, D. S., & Gómez-Pujol, L. (2020). Coastal impacts of Storm Gloria (January 2020) over the north-western Mediterranean. *Natural Hazards and Earth System Sciences*, *20*(7), 1955–1968. https://doi.org/10.5194/nhess-20-1955-2020

Backhaus, J. O. (1985). A three-dimensional model for the simulation of shelf sea dynamics. *Deutsche Hydrographische Zeitschrift*, *38*(4), 165–187. https://doi.org/10.1007/BF02328975

633 Booij, N., & Holthuijsen, L. H. (1987). Propagation of ocean waves in discrete spectral wave
634 models. *Journal of Computational Physics*, *68*(2), 307–326.
635 https://doi.org/10.1016/0021-9991(87)90060-X
636 Calafat, F. M., Avgoustoglou, E., Jordà, G., Flocas, H., Zodiatis, G., Tsimplis, M. N., &
637 Kouroutzoglou, J. (2014). The ability of a barotropic model to simulate sea level
638 extremes of meteorological origin in the Mediterranean Sea, including those caused by
639 explosive cyclones. *Journal of Geophysical Research: Oceans*, *119*(11), 7840–7853.
640 https://doi.org/10.1002/2014JC010360
641 Calafat, F. M., Gomis, D., & Marcos, M. (2009). Comparison of Mediterranean sea level fields
642 for the period 1961–2000 as given by a data reconstruction and a 3D model. *Global and*
643 *Planetary Change*, *68*(3), 175–184. https://doi.org/10.1016/j.gloplacha.2009.04.003
644 Callahan, J. A., & Leathers, D. J. (2021). Estimation of Return Levels for Extreme Skew Surge
645 Coastal Flooding Events in the Delaware and Chesapeake Bays for 1980–2019. *Frontiers*
646 *in Climate*, *3*, 684834. https://doi.org/10.3389/fclim.2021.684834
647 Cherif, S., Doblas-Miranda, E., Lionello, P., Borrego, C., Giorgi, F., Iglesias, A., Jebari, S.,
648 Mahmoudi, E., Moriondo, M., Pringault, O., Rilov, G., Somot, S., Tsikliras, A., Vila, M.,
649 & Zittis, G. (2020). Drivers of Change. In W. Cramer, J. Guiot, & K. Marini (Eds.),
650 *Climate and Environmental Change in the Mediterranean Basin – Current Situation and*
651 *Risks for the Future. First Mediterranean Assessment Report* (pp. 59–180). Union for the
652 Mediterranean, Plan Bleu, UNEP/MAP. 10.5281/zenodo.7100601
653 Cid, A., Menéndez, M., Castanedo, S., Abascal, A. J., Méndez, F. J., & Medina, R. (2016).
654 Long-term changes in the frequency, intensity and duration of extreme storm surge
655 events in southern Europe. *Climate Dynamics*, *46*(5–6), 1503–1516.
656 https://doi.org/10.1007/s00382-015-2659-1
657 Codiga, D. (2023). UTide Unified Tidal Analysis and Prediction Functions. [Software].
658 Mathworks. https://www.mathworks.com/matlabcentral/fileexchange/46523-utide-
659 unified-tidal-analysis-and-prediction-functions
660 de Alfonso, M., Lin-Ye, J., García-Valdecasas, J. M., Pérez-Rubio, S., Luna, M. Y., Santos-
661 Muñoz, D., Ruiz, M. I., Pérez-Gómez, B., & Álvarez-Fanjul, E. (2021). Storm Gloria:
662 Sea State Evolution Based on in situ Measurements and Modeled Data and Its Impact on

Extreme Values. *Frontiers in Marine Science*, *8*, 646873. https://doi.org/10.3389/fmars.2021.646873

Del-Rosal-Salido, J., Folgueras, P., Bermúdez, M., Ortega-Sánchez, M., & Losada, M. Á. (2021). Flood management challenges in transitional environments: Assessing the effects of sea-level rise on compound flooding in the 21st century. *Coastal Engineering*, *167*, 103872. https://doi.org/10.1016/j.coastaleng.2021.103872

Dey, A. K., & Das, K. P. (2016). Modeling Extreme Hurricane Damage Using the Generalized Pareto Distribution. *American Journal of Mathematical and Management Sciences*, *35*(1), 55–66. https://doi.org/10.1080/01966324.2015.1075926

Dodet, G., Melet, A., Ardhuin, F., Bertin, X., Idier, D., & Almar, R. (2019). The Contribution of Wind-Generated Waves to Coastal Sea-Level Changes. *Surveys in Geophysics*, *40*(6), 1563–1601. https://doi.org/10.1007/s10712-019-09557-5

Dupuis, D. J. (1999). Exceedances over High Thresholds: A Guide to Threshold Selection. *Extremes*, *1*, 251–261. https://doi.org/10.1023/A:1009914915709

Enríquez, A. R. (2022). MatFlood. [Software]. Zenodo. https://doi.org/10.5281/zenodo.7448967

Enríquez, A. R., Wahl, T., Marcos, M., & Haigh, I. D. (2020). Spatial Footprints of Storm Surges Along the Global Coastlines. *Journal of Geophysical Research: Oceans*, *125*(9). https://doi.org/10.1029/2020JC016367

Eurotop, Van der Meer, J. W., Allsop, N. W. H., Bruce, T., De Rouck, J., Kortenhaus, A., Pullen, T., Schüttrumpf, H., Troch, P., & Zanuttigh, B. (2018). *Manual on wave overtopping of sea defences and related structures. An overtopping manual largely based on European research, but for worldwide application*. www.overtopping-manual.com

Ferrarin, C., Bellafiore, D., Sannino, G., Bajo, M., & Umgiesser, G. (2018). Tidal dynamics in the inter-connected Mediterranean, Marmara, Black and Azov seas. *Progress in Oceanography*, *161*, 102–115. https://doi.org/10.1016/j.pocean.2018.02.006

Fiedler, J. W., Smit, P. B., Brodie, K. L., McNinch, J., & Guza, R. T. (2018). Numerical modeling of wave runup on steep and mildly sloping natural beaches. *Coastal Engineering*, *131*, 106–113. https://doi.org/10.1016/j.coastaleng.2017.09.004

García-Valdecasas, J., Pérez Gómez, B., Molina, R., Rodríguez, A., Rodríguez, D., Pérez, S., Campos, Á., Rodríguez Rubio, P., Gracia, S., Ripollés, L., Terrés Nicoli, J. M., de los Santos, F. J., & Álvarez Fanjul, E. (2021). *Operational tool for characterizing high*

frequency sea level oscillations. *106*, 1149–1167. https://doi.org/10.3989/scimar.2001.65s1145

Gomis, D., Tsimplis, M., Marcos, M., Fenoglio-Marc, L., Pérez, B., Raicich, F., Vilibić, I., Wöppelmann, G., & Monserrat, S. (2012). Mediterranean Sea-Level Variability and Trends. In P. Lionello (Ed.), *The Climate of the Mediterranean Region* (pp. 257–299). Elsevier. https://doi.org/10.1016/B978-0-12-416042-2.00004-5

Haigh, I. D., Wadey, M. P., Wahl, T., Ozsoy, O., Nicholls, R. J., Brown, J. M., Horsburgh, K., & Gouldby, B. (2016). Spatial and temporal analysis of extreme sea level and storm surge events around the coastline of the UK. *Scientific Data*, *3*(1), 160107. https://doi.org/10.1038/sdata.2016.107

Hasselmann, S., Hasselmann, K., Bauer, E., Janssen, P. A. E., Komen, G. J., Bertotti, L., Lionello, P., Guillaume, A., Cardone, V. C., Greenwood, J. A., Reistad, M., Zambresky, L., & Ewing, J. A. (1988). The WAM Model—A Third Generation Ocean Wave Prediction Model. *Journal of Physical Oceanography*, *18*(12), 1775–1810.

Holthuijsen, L. H. (2007). *Waves in Oceanic and Coastal Waters*.

Horsburgh, K. J., & Wilson, C. (2007). Tide-surge interaction and its role in the distribution of surge residuals in the North Sea. *Journal of Geophysical Research*, *112*(C8), C08003. https://doi.org/10.1029/2006JC004033

Huthnance, J. M., Mysak, L. A., & Wang, D.-P. (1986). Coastal trapped waves. In C. N. K. Mooers (Ed.), *Coastal and Estuarine Sciences* (Vol. 3, pp. 1–18). American Geophysical Union. https://doi.org/10.1029/CO003p0001

Lambert, E., Rohmer, J., Le Cozannet, G., & van de Wal, R. S. W. (2020). Adaptation time to magnified flood hazards underestimated when derived from tide gauge records. *Environmental Research Letters*, *15*(7), 074015. https://doi.org/10.1088/1748-9326/ab8336

Larnicol, G., Ayoub, N., & Le Traon, P. Y. (2002). Major changes in Mediterranean Sea level variability from 7 years of TOPEX/Poseidon and ERS-1/2 data. *Journal of Marine Systems*, *33–34*, 63–89. https://doi.org/10.1016/S0924-7963(02)00053-2

Marcos, M., Tsimplis, M. N., & Shaw, A. G. P. (2009). Sea level extremes in southern Europe. *Journal of Geophysical Research*, *114*(C1), C01007. https://doi.org/10.1029/2008JC004912

Marcos, M., & Woodworth, P. L. (2017). Spatiotemporal changes in extreme sea levels along the coasts of the N orth A tlantic and the G ulf of M exico. *Journal of Geophysical Research: Oceans*, *122*(9), 7031–7048. https://doi.org/10.1002/2017JC013065

Melet, A., Meyssignac, B., Almar, R., & Le Cozannet, G. (2018). Under-estimated wave contribution to coastal sea-level rise. *Nature Climate Change*, *8*(3), 234–239. https://doi.org/10.1038/s41558-018-0088-y

Menéndez, M., & Woodworth, P. L. (2010). Changes in extreme high water levels based on a quasi-global tide-gauge data set. *Journal of Geophysical Research: Oceans*, *115*(C10), 2009JC005997. https://doi.org/10.1029/2009JC005997

Middleton, J. F., & Thompson, K. R. (1986). Return periods of extreme sea levels from short records. *Journal of Geophysical Research*, *91*(C10), 11707. https://doi.org/10.1029/JC091iC10p11707

Monserrat, S., Vilibić, I., & Rabinovich, A. B. (2006). Meteotsunamis: Atmospherically induced destructive ocean waves in the tsunami frequency band. *Natural Hazards and Earth System Sciences*, *6*(6), 1035–1051. https://doi.org/10.5194/nhess-6-1035-2006

Muis, S., Verlaan, M., Winsemius, H. C., Aerts, J. C. J. H., & Ward, P. J. (2016). A global reanalysis of storm surges and extreme sea levels. *Nature Communications*, *7*(1), 11969. https://doi.org/10.1038/ncomms11969

Nicholls, R. J., Hanson, S. E., Lowe, J. A., Warrick, R. A., Lu, X., & Long, A. J. (2014). Sea-level scenarios for evaluating coastal impacts. *WIREs Climate Change*, *5*(1), 129–150. https://doi.org/10.1002/wcc.253

Noji, E. K. (1991). Natural Disasters. *Critical Care Clinics*, *7*(2), 271–292. https://doi.org/10.1016/S0749-0704(18)30306-3

Pérez, B., Álvarez Fanjul, E., Pérez, S., de Alfonso, M., & Vela, J. (2013). Use of tide gauge data in operational oceanography and sea level hazard warning systems. *Journal of Operational Oceanography*, *6*(2), 1–18. https://doi.org/10.1080/1755876X.2013.11020147

Pérez Gómez, B., Vilibić, I., Šepić, J., Međugorac, I., Ličer, M., Testut, L., Fraboul, C., Marcos, M., Abdellaoui, H., Álvarez Fanjul, E., Barbalić, D., Casas, B., Castaño-Tierno, A., Čupić, S., Drago, A., Fraile, M. A., Galliano, D. A., Gauci, A., Gloginja, B., … Zodiatis,

G. (2022). Coastal sea level monitoring in the Mediterranean and Black seas. *Ocean Science*, *18*(4), 997–1053. https://doi.org/10.5194/os-18-997-2022

Pilar, P., Soares, C. G., & Carretero, J. C. (2008). 44-year wave hindcast for the North East Atlantic European coast. *Coastal Engineering*, *55*(11), 861–871. https://doi.org/10.1016/j.coastaleng.2008.02.027

Rabinovich, A. B. (2020). Twenty-Seven Years of Progress in the Science of Meteorological Tsunamis Following the 1992 Daytona Beach Event. *Pure and Applied Geophysics*, *177*(3), 1193–1230. https://doi.org/10.1007/s00024-019-02349-3

Raby, A. (2003). *Extreme Waves, Overtopping and Flooding at Sea Defences* [University of Oxford]. https://ora.ox.ac.uk/objects/uuid:82fcc770-8838-4f9b-9abe-32eecdd05f9a

Ramos-Alcántara, J., Agulles, M., Villalonga, J., Gomis, D., & Jordà, G. (2023). Sea Level Extremes Analysis [Software]. Zenodo. https://doi.org/10.5281/zenodo.7848818

Rasmussen, C. E., & Williams, C. K. I. (2008). *Gaussian processes for machine learning* (3. print). MIT Press.

Reek, T., Doty, S. R., & Owen, T. W. (1992). A Deterministic Approach to the Validation of Historical Daily Temperature and Precipitation Data from the Cooperative Network. *Bulletin of the American Meteorological Society*, *73*(6), 753–762. https://doi.org/10.1175/1520-0477(1992)073<0753:ADATTV>2.0.CO;2

Ruggiero, P., Komar, P. D., McDougal, W. G., Marra, J. J., & Beach, R. A. (2001). Wave Runup, Extreme Water Levels and the Erosion of Properties Backing Beaches. *Journal of Coastal Research*, *17*(2), 407–419.

Sayol, J. M., & Marcos, M. (2018). Assessing Flood Risk Under Sea Level Rise and Extreme Sea Levels Scenarios: Application to the Ebro Delta (Spain). *Journal of Geophysical Research: Oceans*, *123*(2), 794–811. https://doi.org/10.1002/2017JC013355

Smyth, G. K. (2005). Numerical Integration. In P. Armitage & T. Colton (Eds.), *Encyclopedia of Biostatistics* (p. b2a14026). John Wiley & Sons, Ltd. https://doi.org/10.1002/0470011815.b2a14026

Soto-Navarro, J., Criado-Aldeanueva, F., García-Lafuente, J., & Sánchez-Román, A. (2010). Estimation of the Atlantic inflow through the Strait of Gibraltar from climatological and in situ data. *Journal of Geophysical Research: Oceans*, *115*(C10), 2010JC006302. https://doi.org/10.1029/2010JC006302

Stockdon, H. F., Holman, R. A., Howd, P. A., & Sallenger, A. H. (2006). Empirical parameterization of setup, swash, and runup. *Coastal Engineering*, *53*(7), 573–588. https://doi.org/10.1016/j.coastaleng.2005.12.005

Tintoré, J., Vizoso, G., Casas, B., Heslop, E., Pascual, A., Orfila, A., Ruiz, S., Martínez-Ledesma, M., Torner, M., Cusí, S., Diedrich, A., Balaguer, P., Gómez-Pujol, L., Álvarez-Ellacuria, A., Gómara, S., Sebastian, K., Lora, S., Beltrán, J. P., Renault, L., … Manriquez, M. (2013). SOCIB: The Balearic Islands Coastal Ocean Observing and Forecasting System Responding to Science, Technology and Society Needs. *Marine Technology Society Journal*, *47*(1), 101–117. https://doi.org/10.4031/MTSJ.47.1.10

Tolman, H. L. (1991). A third-generation model for wind waves on slowly varying, unsteady, and inhomogeneous depths and currents. *Journal of Physical Oceanography*, *21*(6), 782–797. https://doi.org/10.1175/1520-0485(1991)021<0782:ATGMFW>2.0.CO;2

Tsimplis, M. N., Calafat, F. M., Marcos, M., Jordà, G., Gomis, D., Fenoglio-Marc, L., Struglia, M. V., Josey, S. A., & Chambers, D. P. (2013). The effect of the NAO on sea level and on mass changes in the Mediterranean Sea: NAO effects on Mediterranean Sea level. *Journal of Geophysical Research: Oceans*, *118*(2), 944–952. https://doi.org/10.1002/jgrc.20078

Tsimplis, M. N., Marcos, M., Pérez, B., Challenor, P., Garcia-Fernandez, M. J., & Raicich, F. (2009). On the effect of the sampling frequency of sea level measurements on return period estimate of extremes—Southern European examples. *Continental Shelf Research*, *29*(18), 2214–2221. https://doi.org/10.1016/j.csr.2009.08.015

Tsimplis, M. N., & Shaw, A. G. P. (2010). Seasonal sea level extremes in the Mediterranean Sea and at the Atlantic European coasts. *Natural Hazards and Earth System Sciences*, *10*(7), 1457–1475. https://doi.org/10.5194/nhess-10-1457-2010

Tsimplis, M. N., & Woodworth, P. L. (1994). The global distribution of the seasonal sea level cycle calculated from coastal tide gauge data. *Journal of Geophysical Research*, *99*(C8), 16031. https://doi.org/10.1029/94JC01115

Vilibić, I., & Šepić, J. (2017). Global mapping of nonseismic sea level oscillations at tsunami timescales. *Scientific Reports*, *7*(1), 40818. https://doi.org/10.1038/srep40818

Vousdoukas, M. I., Wziatek, D., & Almeida, L. P. (2012). Coastal vulnerability assessment based on video wave run-up observations at a mesotidal, steep-sloped beach. *Ocean Dynamics*, *62*(1), 123–137. https://doi.org/10.1007/s10236-011-0480-x

Wahl, T., Haigh, I. D., Nicholls, R. J., Arns, A., Dangendorf, S., Hinkel, J., & Slangen, A. B. A. (2017). Understanding extreme sea levels for broad-scale coastal impact and adaptation analysis. *Nature Communications*, *8*(1), 16075. https://doi.org/10.1038/ncomms16075

Weatherall, P., Marks, K. M., Jakobsson, M., Schmitt, T., Tani, S., Arndt, J. E., Rovere, M., Chayes, D., Ferrini, V., & Wigley, R. (2015). A new digital bathymetric model of the world's oceans. *Earth and Space Science*, *2*(8), 331–345. https://doi.org/10.1002/2015EA000107

Williams, J., Matthews, A., & Jevrejeva, S. (2019). Development of an automatic tide gauge processing system. *National Oceanography Centre Research and Consultancy Report*, *64*, 26.

Wilson, A. G., & Adams, R. P. (2013). Gaussian Process Kernels for Pattern Discovery and Extrapolation. *Proceedings of the 30th International Conference on Machine Learning*, *28*(3), 1067–1075.

Wolf, J. (2009). Coastal flooding: Impacts of coupled wave–surge–tide models. *Natural Hazards*, *49*(2), 241–260. https://doi.org/10.1007/s11069-008-9316-5

Woodworth, P. L., Melet, A., Marcos, M., Ray, R. D., Wöppelmann, G., Sasaki, Y. N., Cirano, M., Hibbert, A., Huthnance, J. M., Monserrat, S., & Merrifield, M. A. (2019). Forcing Factors Affecting Sea Level Changes at the Coast. *Surveys in Geophysics*, *40*(6), 1351–1397. https://doi.org/10.1007/s10712-019-09531-1